



저작자표시-비영리-변경금지 2.0 대한민국

이용자는 아래의 조건을 따르는 경우에 한하여 자유롭게

- 이 저작물을 복제, 배포, 전송, 전시, 공연 및 방송할 수 있습니다.

다음과 같은 조건을 따라야 합니다:



저작자표시. 귀하는 원저작자를 표시하여야 합니다.



비영리. 귀하는 이 저작물을 영리 목적으로 이용할 수 없습니다.



변경금지. 귀하는 이 저작물을 개작, 변형 또는 가공할 수 없습니다.

- 귀하는, 이 저작물의 재이용이나 배포의 경우, 이 저작물에 적용된 이용허락조건을 명확하게 나타내어야 합니다.
- 저작권자로부터 별도의 허가를 받으면 이러한 조건들은 적용되지 않습니다.

저작권법에 따른 이용자의 권리는 위의 내용에 의하여 영향을 받지 않습니다.

이것은 [이용허락규약\(Legal Code\)](#)을 이해하기 쉽게 요약한 것입니다.

[Disclaimer](#)

Master's Thesis

Molecular Engineering for Enhancement of
Thermal/Light/Water Stability of Organic Dyes for
Dye-Sensitized Solar Cells

Un-Young Kim

Department of Chemistry

Graduate School of UNIST

2018

Molecular Engineering for Enhancement of
Thermal/Light/Water Stability of Organic Dyes
for Dye-Sensitized Solar Cells

Un-Young Kim

Department of Chemistry

Graduate School of UNIST

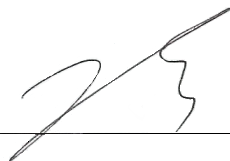
Molecular Engineering for Enhancement of Thermal/Light/Water Stability of Organic Dyes for Dye-Sensitized Solar Cells

A thesis
submitted to the Graduate School of UNIST
in partial fulfillment of the
requirements for the degree of
Master of Science

Un-Young Kim

12 / 13 / 2017

Approved by



Advisor

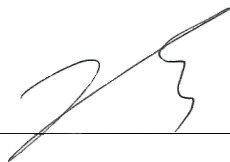
Tae-Hyuk Kwon

Molecular Engineering for Enhancement of Thermal/Light/Water Stability of Organic Dyes for Dye-Sensitized Solar Cells

Un-Young Kim

This certifies that the thesis of Un-Young Kim is approved.

12/13/2017



Advisor: Tae-Hyuk Kwon



Young S. Park



Cheol-Min Park

Abstract

Ru-based sensitizers (N719, N3, black dye, etc.) have been developed continuously and reached an efficiency of ~11.7% under AM 1.5G irradiation (1000 W/m²). However, these Ru-based sensitizers are not adequate to commercialization because of a stability issue and a need of thick TiO₂ film for a high power conversion efficiency (PCE). Therefore, we designed and synthesized total four organic sensitizers by varying functional groups on donor moieties to understand the structure-property relationship of the solar cell devices, ranging from the stability to the efficiency in thin TiO₂ film system. First, all the sensitizers were composed of dithieno[3,2-b:2',3'-d]thiophene (DTT) as a π -conjugated bridge for a strong stability against external environment. Second, three sensitizers (TP-1, TP-2 and TP-3) contained the proton (control group), the methoxy group, and the carbazole group on donor moieties respectively. TP-2 with methoxy groups achieved the highest PCE of 8.70% and exhibited stronger thermal and light stability than TP-1 and TP-3 which can be attributed to the good electron donating ability. However, TP-2 showed the lowest water stability. On the other hands, TP-3 with carbazole groups showed a relatively low PCE of 7.40%. TP-3 also exhibited weak thermal and light stability because 3,6-position of carbazole were easily oxidized by external energy but achieved the highest water stability presumably by the strong hydrophobicity of carbazole groups. Based on the observation, we postulated protecting role of functional groups on donors (TPA) and themselves was vital to determine the stability. Therefore, TP-4 with a 2-ethylhexyloxy group was designed and synthesized for protecting oxygen on alkoxy group. As a result, TP-4 achieved high stabilities in terms of thermal, light and water stability and a PCE as high as 7.80% due to the strong electron donating ability as shown in the methoxy group of TP-2.

Contents

I. Introduction.....	1
1.1 Dye-sensitized Solar Cells (DSCs)	1
1.1.1 The advancement of DSCs.....	1
1.1.2 Structure and mechanism of DSCs	2
1.1.3 The characteristics of DSCs	3
1.2 Types of dyes in DSCs	5
1.2.1 Metal dyes	6
1.2.2 Metal-free organic dyes.....	7
II. Result and Discussion	9
2.1 Synthesis of TP-series.....	9
2.2 Photophysical and electrochemical properties	11
2.3 Density functional theory (DFT) calculations.....	13
2.4 Device performance	14
2.4.1 Light harvesting efficiency	16
2.4.2 Charge injection efficiency	16
2.4.3 Charge regeneration efficiency	18
2.4.4 Charge collection efficiency.....	20
2.4.5 Electrochemical impedance spectroscopy (EIS) analysis	21
2.5 Stability test	22
2.5.1 Thermal stability	22
2.5.2 Light stability	23
2.5.3 Water stability	25
III. Experimental method	27
3.1 Synthesis : TP-series dyes and Bestmann-reagent	27
3.2 Device Fabrication	45
3.2.1 DSC device fabrication	45
3.2.2 Electrolyte fabrication.....	46
IV. Conclusion.....	47
V. Reference.....	48
VI. Acknowledgement.....	51

List of Figures

- Figure 1.1** Best cell efficiencies depending on the kinds of PV.
- Figure 1.2** Structure and mechanism of Dye-sensitized Solar Cell.
- Figure 1.3** Overview of processes and typical time constants under working conditions (1 SUN) in a Ru-dye-sensitized solar cell with iodide/triiodide electrolyte. Recombination processes are marked with red arrows.
- Figure 1.4** Schematic J - V curve and parameters of a DSC device.
- Figure 1.5** Redox potentials of diverse electrolytes and relative energy level of dye and TiO_2 conduction band.
- Figure 1.6** Representative donor and π -conjugation derivatives and schematic diagram of intramolecular charge transfer (ICT).
- Figure 1.7** Structures of various Ru-based dye molecules.
- Figure 1.8** Structures of various metal-free organic dyes.
- Figure 2.1** Synthesis of π -bridge and donor units.
- Figure 2.2** Synthesis of the four dyes (TP-1, TP-2, TP-3 and TP-4) by coupling reaction and condensation reaction.
- Figure 2.3** (a) Absorption spectra of TP-series in dichloromethane (0.02mM), (b) absorption spectra of TP-series adsorbed onto TiO_2 film, (c) cyclic voltammetry of TP series and ferrocene, and (d) energy levels of TP-series, TiO_2 conduction band and I_3^-/I^- .
- Figure 2.4** HOMO and LUMO of TP-series estimated by DFT calculation.
- Figure 2.5** (a) J - V curve of TP-series with liquid electrolyte and (b) J - V curve of TP-series with ionic liquid electrolyte under AM 1.5G illumination (1000 W/m^2).
- Figure 2.6** LHE of TP-series on thin photoelectrodes
- Figure 2.7** Time-correlated single photon counting (TCSPC) of TP series (a) on TiO_2 1.8 μm layer and (b) on ZrO_2 films : 448.4 nm excitation and 689.4 nm detection.
- Figure 2.8** Time-correlated single photon counting (TCSPC) of TP-series with iodine electrolyte and without electrolyte.
- Figure 2.9** (a) Transport times of TP series and (b) electron life-time according to light intensity by IMPS and IMVS. (c) Charge collection efficiency calculated by transport time and electron life-time.
- Figure 2.10** Nyquist plot of TP-series measured by electrochemical impedance spectroscopy (EIS) under the dark condition.
- Figure 2.11** The photovoltaic parameters of TP-series with ionic liquid electrolyte at 70°C under dark condition.

Figure 2.12 Normalized UV absorbance of (a) TP-1, (b) TP-2, (c) TP-3, (d) TP-4 and (e) N719 on TiO₂ film according to light soaking time.

Figure 2.13 FT-IR spectra of ID1 and RK-2 after 2 hours 1 SUN light soaking.

Figure 2.14 Normalized UV absorbance of (a) TP-1, (b) TP-2, (c) TP-3 and (d) TP-4 on TiO₂ film according to submersion time.

Figure 3.1 ¹H NMR of **D-1** in CDCl₃

Figure 3.2 ¹³C NMR of **D-1** in CDCl₃

Figure 3.3 ¹H NMR of **D-2** in CDCl₃

Figure 3.4 ¹³C NMR of **D-2** in CDCl₃

Figure 3.5 ¹H NMR of **D-3** in CDCl₃

Figure 3.6 ¹H NMR of **D-4** in CDCl₃

Figure 3.7 ¹³C NMR of **D-4** in CDCl₃

Figure 3.8 ¹H NMR of **EF-1** in CDCl₃

Figure 3.9 ¹³C NMR of **EF-1** in CDCl₃

Figure 3.10 ¹H NMR of **EF-2** in CDCl₃

Figure 3.11 ¹³C NMR of **EF-2** in CDCl₃

Figure 3.12 ¹H NMR of **EF-3** in CDCl₃

Figure 3.13 ¹H NMR of **TP-1** in DMSO/CDCl₃

Figure 3.14 ¹³C NMR of **TP-1** in DMSO/CDCl₃

Figure 3.15 ¹H NMR of **TP-2** in DMSO/CDCl₃

Figure 3.16 ¹³C NMR of **TP-2** in DMSO/CDCl₃

Figure 3.17 ¹H NMR of **TP-3** in DMSO/CDCl₃

Figure 3.18 ¹³C NMR of **TP-3** in DMSO/CDCl₃

Figure 3.19 ¹H NMR of **TP-4** in DMSO/CDCl₃

List of Tables

Table 2.1 Photophysical and electrochemical properties of TP-series.

Table 2.2 Photovoltaic parameters of TP-series with liquid and ionic liquid electrolyte.

Table 2.3 τ_{inj} on TiO_2 and τ_{inj} on ZrO_2 by Time-Correlated Single Photon Counting (TCSPC) of TP-series.

Table 2.4 Time-Correlated Single Photon Counting (TCSPC) of TP-series on ZrO_2 with iodine electrolyte and without iodine electrolyte.

I. Introduction

1.1 Dye-sensitized Solar Cells (DSCs)

1.1.1 The advancement of DSCs

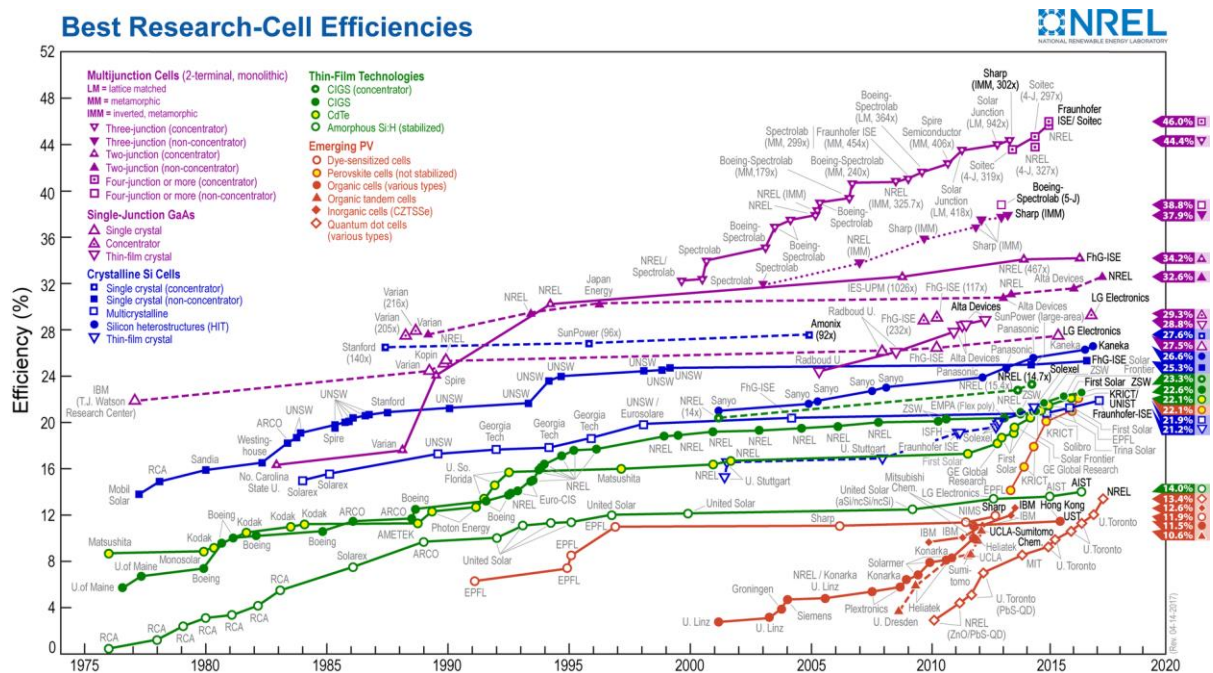


Figure 1.1 Best cell efficiencies depending on the kinds of PV.¹

As global energy depletion problem and an interest in environmental pollution have been increased, researches on the development of eco-friendly energy generating system have become more important. For this reason, photovoltaics (PV) which convert light into electricity using photovoltaic effect have been developed and as a result, forms of PV (Si solar cells, polymer solar cells, perovskite cells, etc.) have been diversified continuously (Figure 1.1).¹ Among the diverse PV, Dye-sensitized Solar Cells (DSCs) was invented by M. Grätzel and B. O'Regan in 1991 using trimeric ruthenium complex and since then, many researches on DSCs have been studied due to unique advantages of DSCs, including high efficiency at low illumination, transparency, available as a flexible device and realization of multiple colors. Because of these features, DSCs are suitable for building-integrated photovoltaics (BIPV), automotive-integrated photovoltaics (AIPV) and portable indoor power generators.²⁻³

1.1.2 Structure and mechanism of DSCs

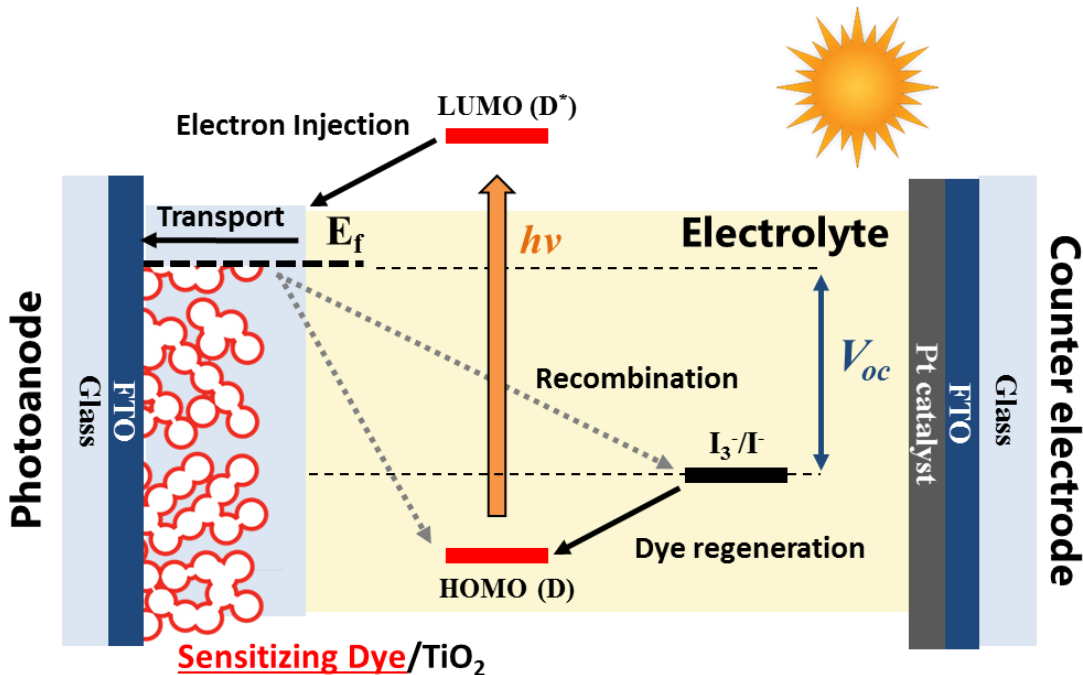


Figure 1.2 Structure and mechanism of Dye-sensitized Solar Cell.

There are five components of Dye-sensitized Solar Cell (DSC) that are (Figure 1.2)

- (1) **Dye** : sensitizer
- (2) **Semiconductor** : TiO_2
- (3) **Electrolyte** : redox mediator (ex. I_3^-/I^-)
- (4) **Mechanical supporter** : FTO glass coated with TiO_2
- (5) **Counter electrode** : Pt

and the mechanism is as follows.

1. Dyes adsorbed on TiO_2 semiconductor are excited by light.
2. The excited electrons of dyes are injected into TiO_2 semiconductor and then dyes are oxidized.
3. The electrons transport to FTO and flow to counter electrode through external circuit.
4. At counter electrode, the electrons reduce the redox mediators (I_3^-/I^-) in electrolyte.
5. Finally, oxidized dyes are regenerated (reduced) by the redox mediators.

However, injected electrons in the semiconductor (step 2) somewhat follow electron recombination with oxidized dyes and redox mediator causing low power conversion efficiency (PCE). In Figure 1.3, the kinetics for a working DSC device shows the life-times of electron on each states. Electron transport time is 10^{-3} s and the electron recombination times, meaning electrons on TiO_2 semiconductor move to oxidized dyes and redox mediator, are 10^{-4} s and 10^{-2} s respectively.⁴⁻⁶ Therefore, it is possible that

electrons on TiO₂ move to oxidized dye or redox mediator. As a result, we need to develop a strategy in which recombination occurs less frequently.

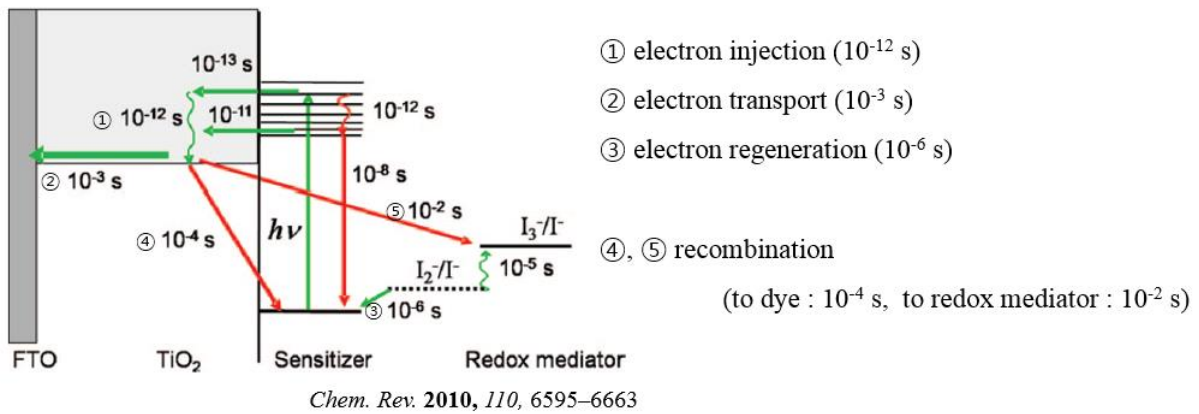


Figure 1.3 Overview of processes and typical time constants under working conditions (1 SUN) in a Ru-dye-sensitized solar cell with iodide/triiodide electrolyte. Recombination processes are marked with red arrows.

1.1.3 The characteristics of DSCs

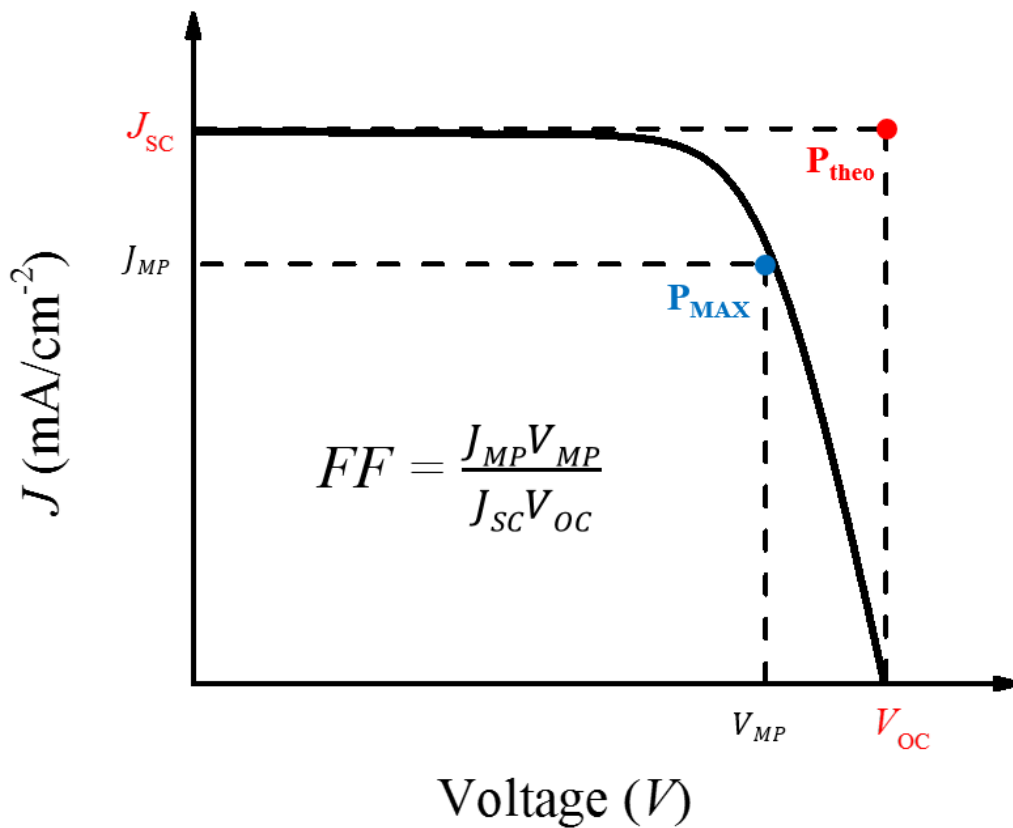


Figure 1.4 Schematic J - V curve and parameters of a DSC device.

For performance evaluation of DSC devices, there are important photovoltaic parameters to be considered. Figure 1.4 shows a J - V curve including the photovoltaic parameters (J_{SC} , V_{OC} and FF). J_{SC} is the short circuit current density (the current density, when cell is operated at $V=0$), V_{OC} is the open circuit voltage (the voltage, when cell is operated at $J=0$), and FF (fill factor) is the ratio of obtainable maximum power (P_{max}) to the theoretical power (P_{theo}). Therefore, power conversion efficiency (PCE or η) is calculated as the ratio of obtainable maximum power (P_{max}) and incident irradiance of a light source (P_{in}) as shown below.⁴

$$\eta = \frac{P_{max}}{P_{in}} \times 100 (\%) = \frac{J_{SC} V_{OC}}{P_{in}} FF \times 100 (\%) \quad \text{equation (1)}$$

Here, J_{SC} is determined by the following equation⁷⁻⁸

$$J_{SC} = q \eta_{lh} \eta_{inj} \eta_{cc} \eta_{reg} I_0 \quad \text{equation (2)}$$

where q is the elementary charge, I_0 is the incident photon flux, η_{lh} is the light harvesting efficiency, η_{inj} is the charge injection efficiency, η_{cc} is the charge collection efficiency, and η_{reg} is the regeneration yield.

V_{OC} is determined by the gap between Fermi level of TiO_2 semiconductor and a redox potential of an electrolyte (Figure 1.2). To improve V_{OC} , representative two kinds of strategies have been conducted. One is use of additives like 4-tert-butylpyridine (TBP) lifting up the TiO_2 conduction band and the other is use of electrolytes with low redox potential like cobalt electrolyte instead of iodine based electrolyte.⁸⁻¹² Since cobalt complex redox mediators have lower redox potential than iodide ions, various researches on cobalt complexes have been conducted (Figure 1.5) and the best performance of 13% with cobalt based electrolyte can be achieved.¹⁰ However, V_{OC} is affected generally by the degree of the charge injection, charge recombination and charge collection. Therefore, V_{OC} have close relation with J_{SC} .

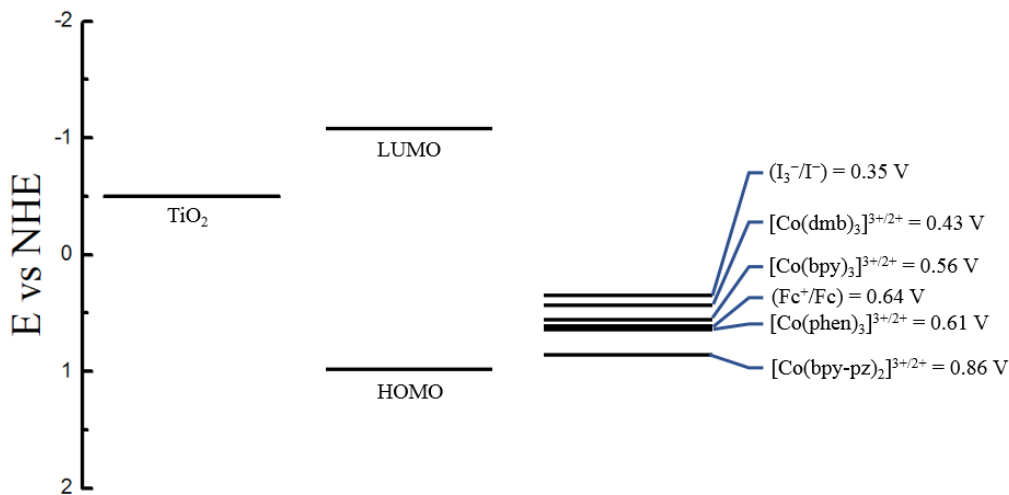


Figure 1.5 Redox potentials of diverse electrolytes and relative energy level of dye and TiO_2 conduction band.

1.2 Types of dyes in DSCs

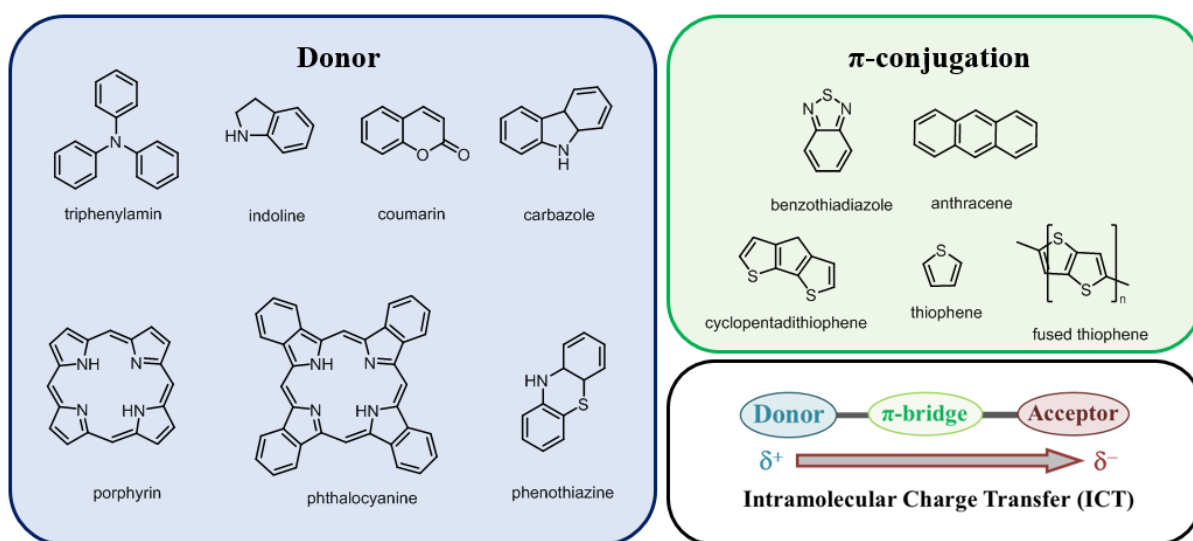


Figure 1.6 Representative donor and π -conjugation derivatives and schematic diagram of intramolecular charge transfer (ICT).

Dyes are very vital component in DSC because dyes absorb light and convert photons into electrons. Depending on the structure of dyes, the absorption wavelength range can be controlled, and photovoltaic parameters like J_{SC} and V_{OC} are affected considerably.

From the $(RuL_2(\mu-(CN)Ru(CN)L'_2)_2)$, where L is 2,2' bipyridine-4,4'-dicarboxylic acid and L' is 2,2'-bipyridine), most of the initial DSC dyes were designed with a Ru (ruthenium metal) such as N3, N719 and black dye.¹³⁻¹⁶ These Ru-based sensitizers showed relatively high PCEs (~9%). However, metal-free organic dyes were developed because Ru-based dyes have poor stability and are expensive and synthetically challenging.¹⁶⁻¹⁸ On the other hands, the organic dyes can be easily synthesized and modified in order to tune the molecular properties. Generally, organic dyes have a donor - π -bridge - acceptor structure to utilize the push-pull effect.¹⁹⁻²² By the push-pull effect, when dye absorb light, the excited electrons in the donor move to the acceptor through π -bridge, and then they are injected into the TiO_2 . Triphenylamin (TPA) derivatives, indoline derivatives, coumarin derivatives, and porphyrin derivatives are commonly used as donor units, while benzothiofene (BT), cyclopentadithiophene and fused thiophene are commonly used in π -bridge.^{10, 23-31} Finally, cyanoacrylic acid and carboxylic acid are used as a anchoring group in acceptor.³² At the beginning of the organic dye development, the organic dyes were less efficient than the Ru-based DSCs, but nowadays there are lots of organic dyes more efficient than the Ru-based DSCs.

1.2.1 Metal dyes

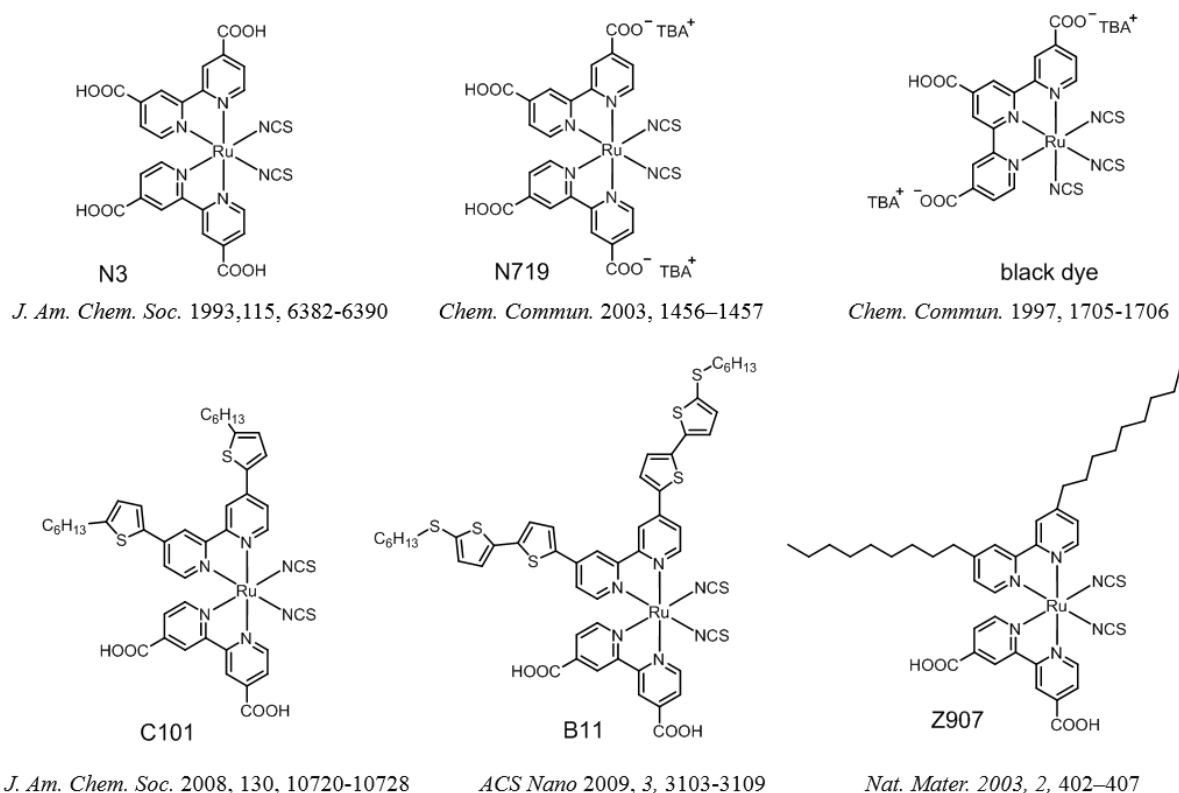


Figure 1.7 Structures of various Ru-based dye molecules.

Early studies for DSCs focused on Ru-based dyes because of the successful demonstration of the first dye, the $(\text{RuL}_2(\mu\text{-}(\text{CN})\text{Ru}(\text{CN})\text{L}'_2)_2)$, where L is 2,2'-bipyridine-4,4'-dicarboxylic acid and L' is 2,2'-bipyridine), was based on Ru.¹³

In order to improve the power conversion efficiency (PCE) from the first Ru-based dye, [2,2'-bipyridine]-4,4'-dicarboxylic acid ligand was introduced to dye molecule (N3) instead of 2,2'-bipyridine-4,4'-dicarboxylic acid and 2,2'-bipyridine of the first dye.¹⁶ The PCE of N3 was 10% under 96.0 mW/cm² and with 10.4 μm TiO₂ film thickness ($J_{\text{SC}}=18.2$ mA/cm², $V_{\text{OC}}=720$ mV and $FF=0.73$). However, four protons on dicarboxylic acids of N3 approached TiO₂ surfaces and lowered TiO₂ conduction band. As a result, photovoltage of N3 tend to be decreased. Therefore, di-tetrabutylammonium cis-bis(isothiocyanato)bis(2,2'-bipyridyl-4,4'-dicarboxylato)ruthenium(II) (N719) was newly developed for preventing protons from lowering TiO₂ conduction band.¹⁴ The initial PCE of N719 is 8.62% under AM 1.5 SUN and with 12 μm TiO₂ film thickness ($J_{\text{SC}}=17.4$ mA/cm², $V_{\text{OC}}=708$ mV, $FF=0.70$). After the advent of N719, N719 has been studied abundantly and have become standard

dye in the DSC field until now. Black dye (trithiocyanato–ruthenium(II) terpyridyl complex) was designed for an efficient panchromatic sensitizer and actually showed broad incident photon to current conversion efficiency (IPCE) up to 920 nm ($J_{SC}=20 \text{ mA/cm}^2$). Another dye Z907 showed relatively high stability against thermal stress and light soaking, whereas Ru-based dyes have weak stability due to thiocyanate (-NCS).¹⁵ The amphiphilic dye Z907 (cis-RuLL'(SCN)₂ (L = 4,4'-dicarboxylic acid-2,2'-bipyridine, L' = 4,4'-dinonyl-2,2'-bipyridine) achieved PCE of >6% with a quasi-solid-state polymer gel electrolyte in AM 1.5 SUN. Surprisingly, Z907 with heating for 1,000 h at 80 °C showed sustained 94% of initial PCE.

Beside above Ru-based dyes, various Ru-based sensitizers have been studied. However, since Ru-based dyes basically contain thiocyanate, they are chemically very unstable. In summary, although Ru-based dyes have shown the relatively high efficiency on thick TiO₂ film (>10 μm) due to low molar extinction co-efficient, new structures of sensitizers need to be developed for solving these problems.

1.2.2 Metal-free organic dyes

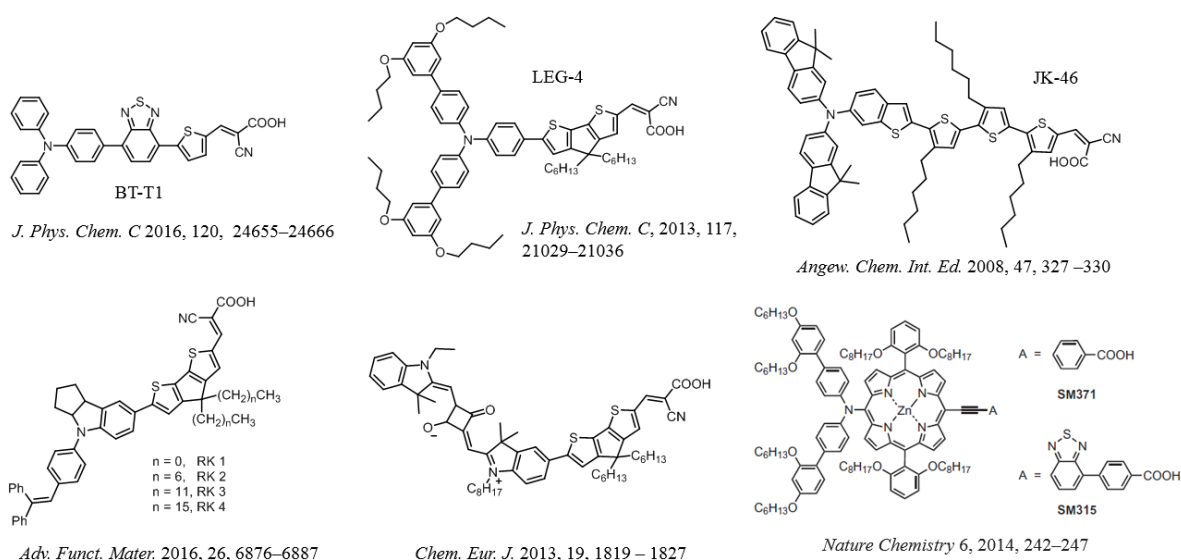


Figure 1.8 Structures of various metal-free organic dyes.

Metal based dyes have several disadvantages : declined PCE value on thin TiO₂ film, usage of transition metal and low stability due to thiocyanate (-NCS). However, organic dyes can resolve these problems due to easiness of modifying molecular structures. Organic dyes are composed of donor - π -

bridge - acceptor in which excited electrons on the donor move to the acceptor through the π conjugation bridge. Therefore, we postulated new dyes in which the stronger electron donating ability is on donor and the stronger electron withdrawing is on acceptor would facilitate intramolecular charge transfer (ICT). In this way, in order to improve ICT on donor moiety : there are two ways

1. By using a donor with strong electron donating ability.
2. By connecting electron donating units to the donor.

Typically, there are a lot of dyes that use triphenylamine (TPA) as a donor.²³ In many cases, triphenylamine (TPA) can be connected with diverse functional groups with strong electron donating ability in order to increase donor's electron donating ability. In addition to TPA, indole or indoline are introduced as a donor moiety because of their good electron donating ability.^{26,33} In the case of indoline containing dyes, they can be designed with a planar structure on the whole, so it is possible to design a dye molecule that achieves high efficiency in thin TiO₂ film.³⁴ Squaraine based dyes express various colors but strong electron withdrawing ability of squaraine causes back electron transfer and self-quenching leading to low PCE.³⁵ Besides, squaraine dyes is damaged fast. In the case of porphyrin containing dyes, they showed overall high PCEs (>8%).²⁸ Indeed, porphyrin based dye, SM 315, achieved the highest PCE of 13% (J_{SC} =18.1 mA/cm², V_{OC} =0.91 V and FF =0.78) when used with a cobalt electrolyte in a single dye condition.¹⁰ However, one problem of porphyrin containing dyes is that it is difficult to synthesize porphyrin and the yield of porphyrin is very low. These are negative aspects commercialization.

Therefore, in my research, we designed and synthesized dye molecules to complement the problems presented above :

1. Low efficiency in thin film system → High efficiency in thin film system.
2. Low stability → High stability on the thermal/light/water.
3. Hard synthesis and low yield → Simple synthesis and valid yield.

with organic dyes. There are two strategies for achieving above three goals : first, dithieno[3,2-*b*:2',3'-*d*]thiophene (DTT) unit was introduced, and second, diverse functional groups with strong donating ability were linked on donor moiety. As a first strategy, DTT having planar and rigid structure showed intense electronic absorption, good hole mobility and high stability.³⁶⁻³⁸ In particular, planar structures increase charge injection efficiency (η_{inj}) efficiently which is key factor to determine J_{SC} in thin film.³⁹ Therefore, DTT was introduced on π -bridge. As a second strategy, diverse functional groups were linked to TPA donor because we anticipated PCE and stability are changed according to characteristics of functional groups on donor moiety. In this way, we designed three dyes based on DTT : TP-1 (proton), TP-2 (methoxy) and TP-3 (carbazole). Later, TP-4 (2-ethylhexyloxy) was designed and synthesized additionally for improving weakness of TP-2 and TP-3.

II. Result and Discussion

2.1 Synthesis of TP-series

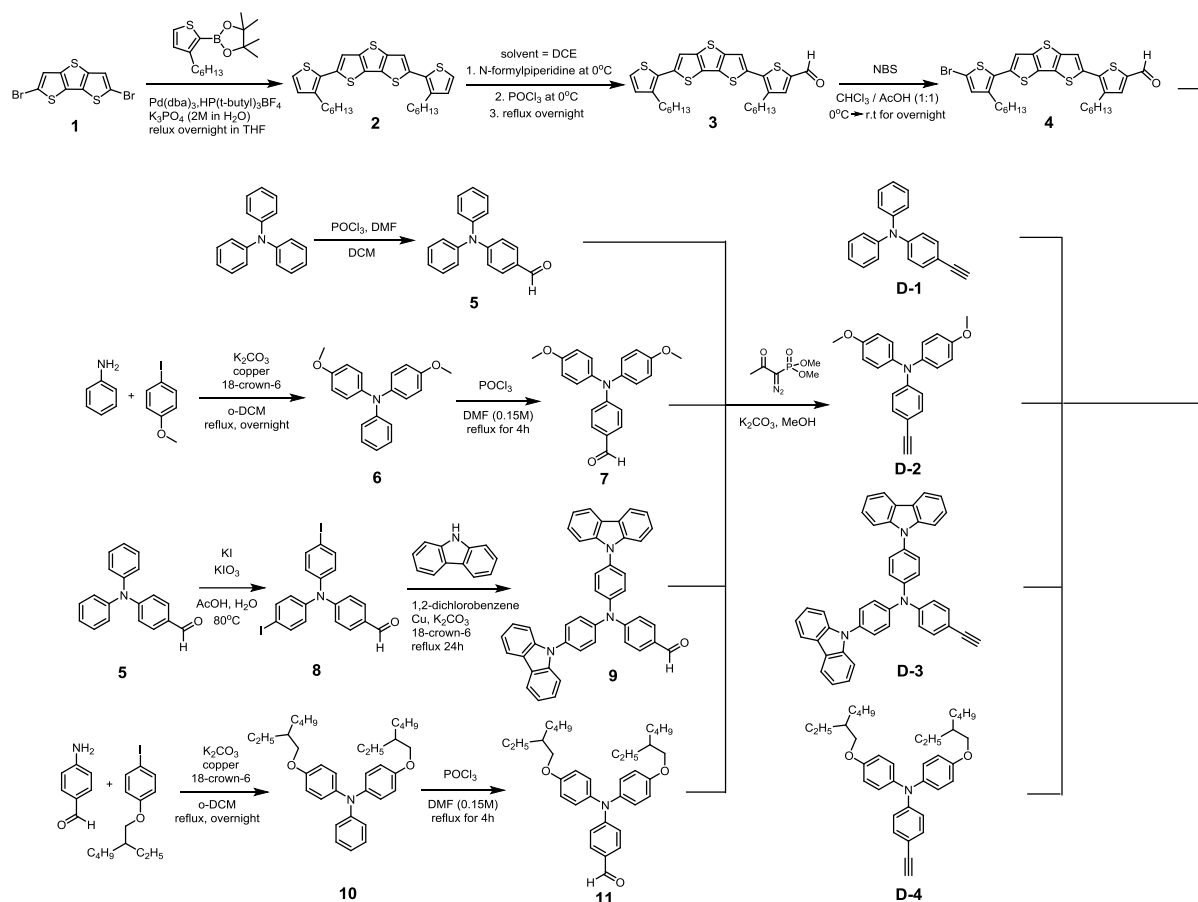


Figure 2.1 Synthesis of π -bridge and donor units.

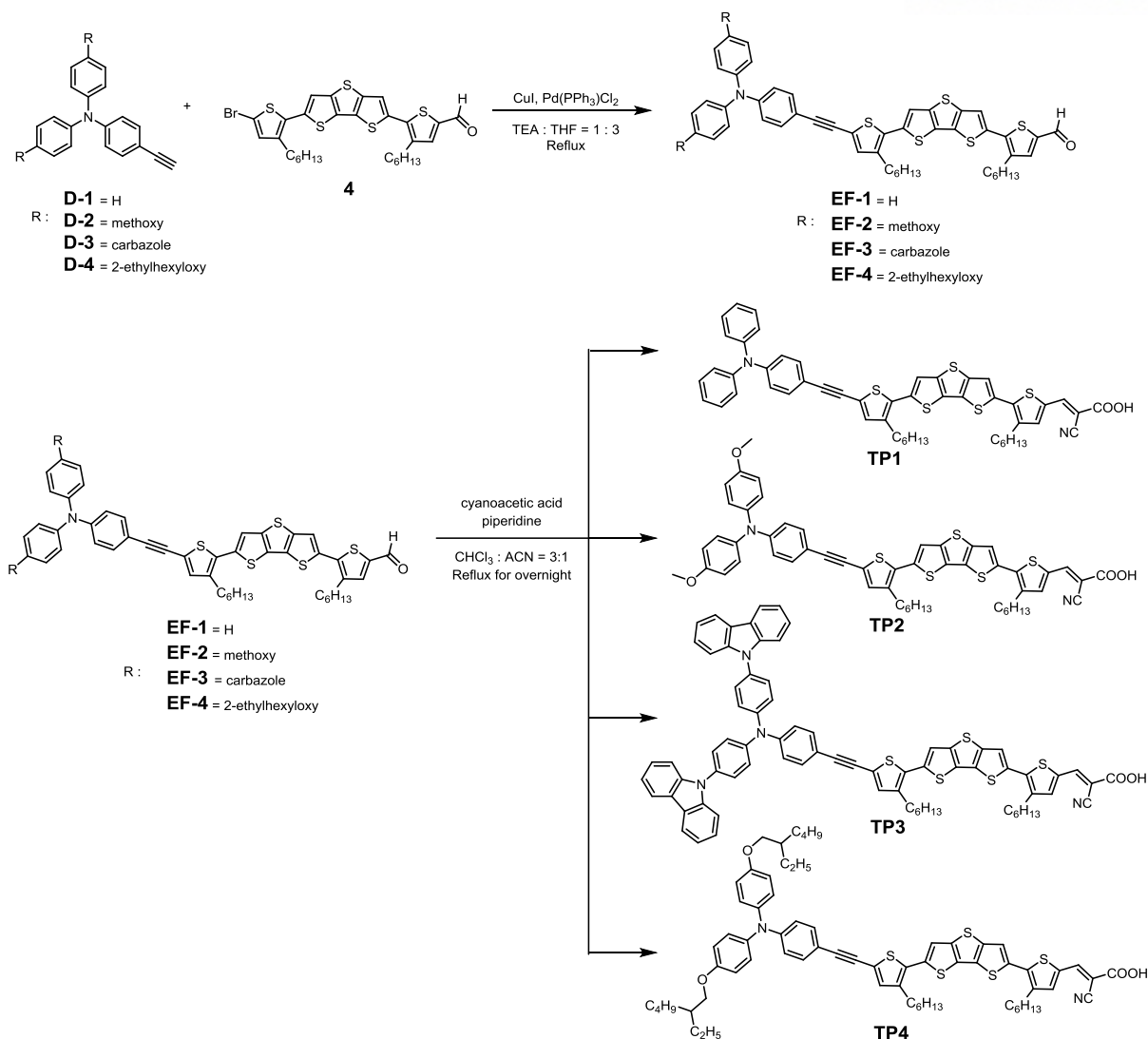


Figure 2.2 Synthesis of the four dyes (TP-1, TP-2, TP-3 and TP-4) by coupling reaction and condensation reaction.

The DTT-based four dyes (TP-1, TP-2, TP-3 and TP-4) were synthesized following Figure 2.1 and 2.2. Figure 2.1 shows the synthetic route of π -bridge and respective donor units. π -bridge, compound 4 (5-(6-(5-bromo-3-hexylthiophen-2-yl)dithieno[3,2-b:2',3'-d]thiophen-2-yl)-4-hexylthiophene-2-carbaldehyde), was obtained from compound 1 (2,6-dibromodithieno[3,2-b:2',3'-d]thiophene)⁴⁰ via the Suzuki-Miyaura cross coupling with 2-(3-hexylthiophen-2-yl)-4,4,5,5-tetramethyl-1,3,2-dioxaborolane followed by Vilsmeier-Haack formylation and NBS bromination. All donor units underwent Vilsmeier-Haack formylation giving aldehyde derivatives which were easily converted into terminal alkyne derivatives using Ohira-Bestmann reagent under mild condition.⁴¹ This Ohira-Bestmann method is very attractive method making aldehyde into terminal alkyne under mild condition in good yield.⁴² Figure

2.2 shows the latter synthetic route. Corresponding donor units with terminal alkyne were coupled with compound 4 (5-(6-(5-bromo-3-hexylthiophen-2-yl)dithieno[3,2-*b*:2',3'-*d*]thiophen-2-yl)-4-hexylthiophene-2-carbaldehyde) under Sonogashira cross coupling reaction.⁴³⁻⁴⁴ In the final step, all target molecules were synthesized via Knoevenagel condensation converting aldehyde on π -conjugated bridge to cyanoacetic acid.

2.2 Photophysical and electrochemical properties

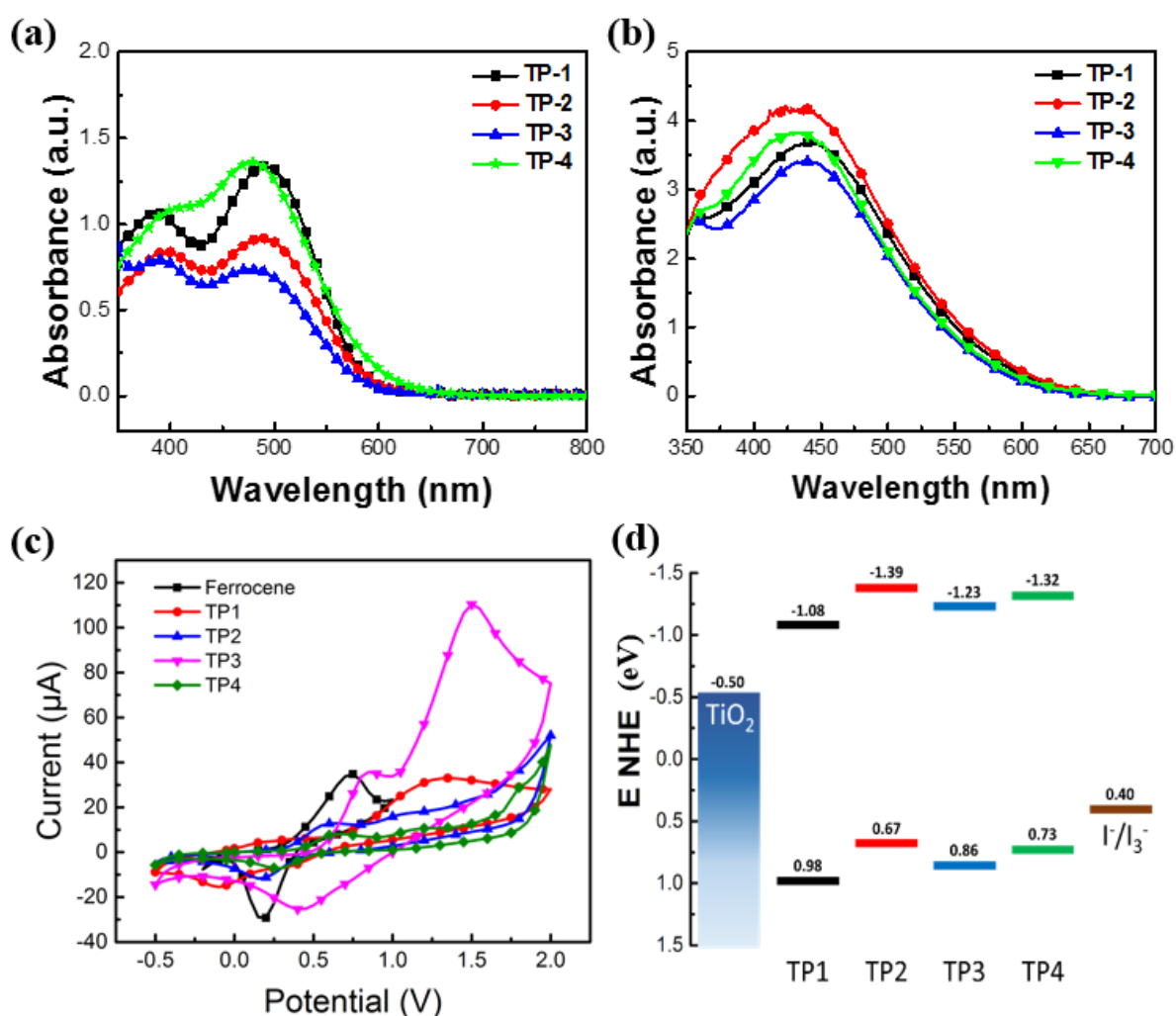


Figure 2.3 (a) Absorption spectra of TP-series in dichloromethane (0.02mM), (b) absorption spectra of TP-series adsorbed onto TiO₂ film, (c) cyclic voltammetry of TP series and ferrocene, and (d) Energy levels of TP-series, TiO₂ conduction band and I₃⁻/I⁻.

Table 2.1 Photophysical and electrochemical properties of TP-series.

Dye	HOMO ^a	LUMO ^b	Abs (nm) ($\epsilon \times 10^4 \text{ cm}^{-1} \text{ M}^{-1}$) ^c	PL (λ_{max})	E _{ox} (V) vs NHE	E _{onset} (V) vs (abs)	E _{ox} - E _{onset} (V)
TP-1	-5.15 eV	-3.09 eV	491(1.34) / 388(1.06)	634	0.98	2.06	-1.08
TP-2	-4.84 eV	-2.78 eV	490(0.91) / 395(0.84)	644	0.67	2.06	-1.39
TP-3	-5.03 eV	-2.94 eV	480(0.73) / 389(0.79)	629	0.86	2.09	-1.23
TP-4	-4.90 eV	-2.93 eV	499(1.19) / 405(1.05)	727	0.73	2.05	-1.32

^aHOMO = $-(E_{\text{ox}} \text{ vs } \text{Fc}^+/\text{Fc}) - 4.8 \text{ eV}$. ^bLUMO = HOMO + E_{onset}. ^cSolvent : dichloromethane (DCM).

The absorption data of TP-series were measured in diluted dichloromethane solution and Figure 2.3a shows the solution absorption data. All of data are summarized in Table 2.1. The four dyes exhibit two absorption band in range of 350 to 450 nm and 450 to 600 nm respectively. The former band is assigned to π - π^* transition and the latter band is assigned to charge transfer (CT) transition. The maximum molar extinction coefficient (ϵ) for the CT transition of TP-series indicates that $\epsilon_{\text{TP1}}=13,400 \text{ cm}^{-1} \text{ M}^{-1}$ at 491 nm, $\epsilon_{\text{TP2}}=9,100 \text{ cm}^{-1} \text{ M}^{-1}$ at 490 nm, $\epsilon_{\text{TP3}}=7,300 \text{ cm}^{-1} \text{ M}^{-1}$ at 480 nm and $\epsilon_{\text{TP4}}=11,900 \text{ cm}^{-1} \text{ M}^{-1}$ at 499 nm. In the case of onset point of the absorption spectra, all of the TP-series have similar λ_{onset} values because it seems λ_{onset} is related to band gap or the energy gap between HOMO and LUMO. Figure 2.3b shows film UV spectroscopy data of TP-series adsorbed onto TiO₂ films. All of TP-series exhibit about 40nm blue-shifts against solution UV absorbance. This result was due to H-aggregation of TP-series molecules onto TiO₂ film. In addition, the degrees of dye aggregation were estimated to be similar by the no change in the degrees of blue-shift.

Figure 2.3d shows the highest occupied molecular orbital (HOMO) and the lowest unoccupied molecular orbital (LUMO) of the TP-series. HOMO was determined by first oxidation potential (E_{ox} vs normal hydrogen electrode (NHE)) measured in cyclic voltammetry (CV) shown in Figure 2.3c and LUMO was obtained by the energy band gap derived from the onset point of UV absorbance. TP-2 and TP-4 have the more negative HOMO than TP-1 and TP-3, ensuring a good donating ability of alkoxy groups. On the other hand, TP-3 exhibits the slight negative shift against TP-2 and TP-4 indicating that carbazole hardly contributes to raising HOMO. This result is because of twisted connection between carbazole groups and TPA donor and the result can be explained by Density functional theory. Finally, HOMOs of TP-series are more positive shift than redox shuttle potential value (0.4 V), assuring that enough driving force lead to regeneration between oxidized dyes and redox shuttle efficiently. Likewise, LUMOs of TP-series are more negative than TiO₂ conduction band, so efficient electron injection processes occur from the excited dyes to TiO₂ conduction.

2.3 Density functional theory (DFT) calculations

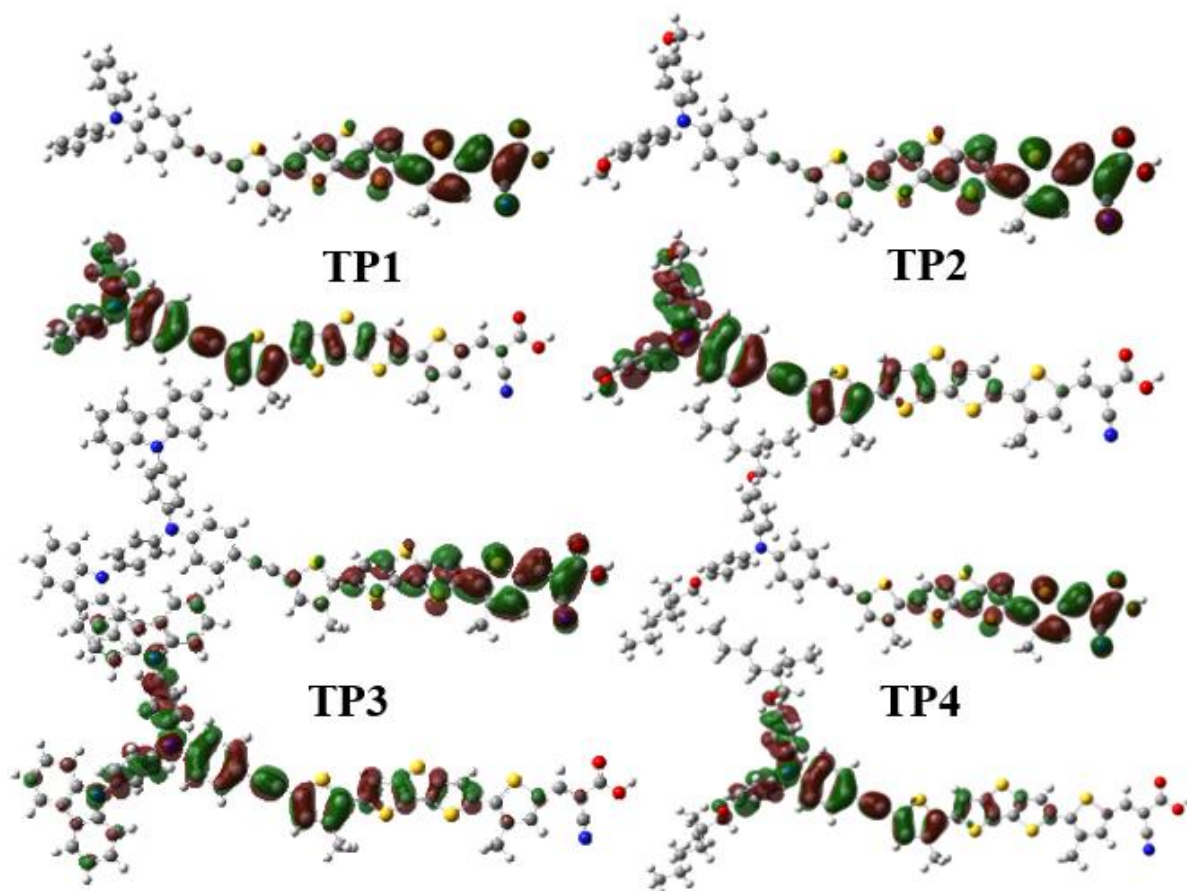


Figure 2.4 HOMO and LUMO of TP-series calculated by DFT calculation.

In Figure 2.4, overall HOMOs of TP-series are delocalized on triphenylamine, dithieno[3,2-*b*:2',3'-*d*]thiophene and 3-hexylthiophene on the donor side while LUMOs are delocalized on dithieno[3,2-*b*:2',3'-*d*]thiophene, 3-hexylthiophene on the acceptor side and cyanoacetic acid. Hence, we can expect efficient intra-molecular charge transfer (ICT) by proper overlap between HOMO and LUMO on dithieno[3,2-*b*:2',3'-*d*]thiophen. Surprisingly, HOMO of TP-3 is not delocalized to carbazole which is in accordance with the low HOMO of TP-3 in Figure 2.3d. Therefore, we concluded carbazole hardly contribute to raise HOMO energy level and this result is because of twisted connection between TP-series and TPA donor shown in HOMO of TP-3.

2.4 Device performance

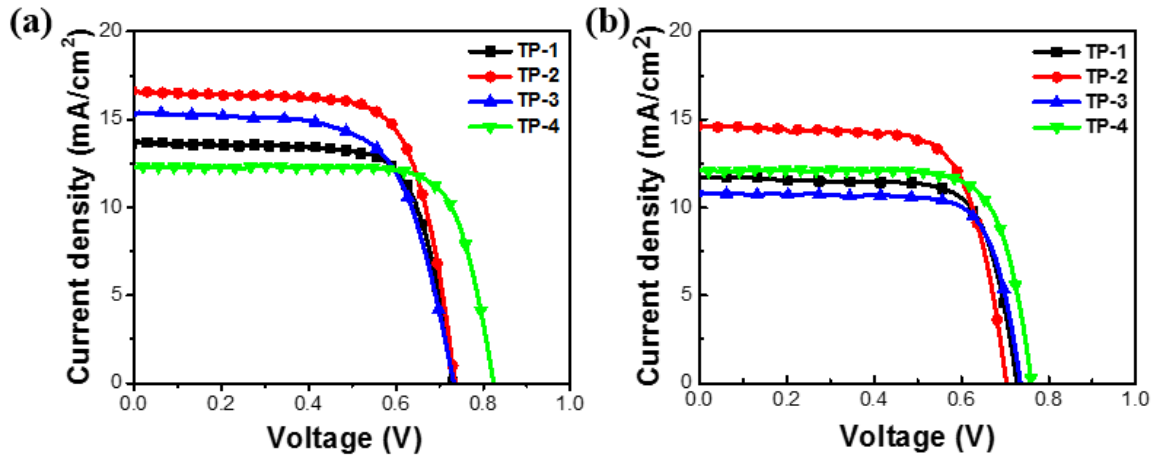


Figure 2.5 (a) J - V curve of TP-series with liquid electrolyte and (b) J - V curve of TP-series with ionic liquid electrolyte under AM 1.5G illumination (1000 W/m^2).

Table 2.2 Photovoltaic parameters of TP-series with liquid and ionic liquid electrolyte

	electrolyte	Film thickness (μm)	J_{SC} (mA cm^{-2})	V_{OC} (V)	FF (%)	η (%)
TP-1	Liquid	3.5(trans)+2.5 (scat)	13.08	0.73	72.4	7.31
TP-2			16.50	0.74	71.6	8.70
TP-3			15.40	0.73	66.3	7.40
TP-4			12.30	0.82	76.9	7.80
TP-1	Ionic	3.5(trans)+2.5(scats)	12.2	0.724	72.7	6.40
TP-2			13.6	0.733	72.9	7.38
TP-3			11.6	0.695	71.3	5.73
TP-4			12.2	0.759	75.0	7.00

Devices were fabricated with liquid electrolyte and ionic liquid electrolyte (ILE) respectively for achieving high PCE and high stability. The both types of DSC devices were measured under AM 1.5G condition (1000 W/m^2). Table 2.2 shows detailed photovoltaic parameters and Figure 2.5 shows the current density-voltage (J - V) curve data of TP-series depending on two kinds of electrolytes. For conventional devices, they were fabricated with thin TiO_2 film ($3.5 \mu\text{m}$ transparent and $2.5 \mu\text{m}$ scattering

layer) and dye solution contained 10 mM chenodeoxycholic acid (CDCA) as the co-adsorbate. In conventional devices, TP-2 exhibits especially the highest PCE of 8.70% ($J_{SC}=16.50 \text{ mA cm}^{-2}$, $V_{OC}=0.74 \text{ V}$ and $FF=71.6$) which is the best performance of DTT based dyes. On the other hands, TP-3 exhibits relatively a low PCE of 7.40% ($J_{SC}=15.40 \text{ mA cm}^{-2}$, $V_{OC}=0.73 \text{ V}$ and $FF=66.3$) than PCE of TP-2. TP-1 shows the lowest PCE among the TP-series ($\eta=7.31\%$, $J_{SC}=13.08 \text{ mA cm}^{-2}$, $V_{OC}=0.73 \text{ V}$ and $FF=72.4$). The PCE of TP-4 ($\eta=7.80\%$, $J_{SC}=12.30 \text{ mA cm}^{-2}$, $V_{OC}=0.82 \text{ V}$ and $FF=0.77$) is higher than PCE of TP-1 and TP-3 but lower than the PCE of TP-2 achieving high photo voltage. Through these data, alkoxy groups (TP-2 and TP-4) shows good donating ability increasing J_{SC} and V_{OC} .

In case of ILE electrolyte based devices, the device characteristics with ILE electrolyte shows similar performance as conventional devices. In ILE devices, TP-2 device shows the best efficiency of 7.38% ($J_{SC}=13.6 \text{ mA cm}^{-2}$, $V_{OC}=0.73 \text{ V}$ and $FF=72.9$) among the TP-series devices. TP-1 ($\eta=6.40\%$, $J_{SC}=12.2 \text{ mA cm}^{-2}$, $V_{OC}=0.724 \text{ V}$ and $FF=72.7$) shows higher PCE than TP-3 ($\eta=5.73\%$, $J_{SC}=11.6 \text{ mA cm}^{-2}$, $V_{OC}=0.695 \text{ V}$ and $FF=71.3$) based on ILE electrolyte devices. The PCE of TP-4 is still lower than TP-2 but shows high photo-voltage. It means that 2-ethylhexyloxy group of TP-4 lowered recombination from redox mediators than other TP-series and increase photo-voltage. In summary, the PCE of TP-series increased in the order TP-1 < TP-3 < TP-4 < TP-2 at conventional but in ILE devices cases, the PCE of TP-series increased in the order TP-3 < TP-1 < TP-4 < TP-2. From these results, functional groups in donor moiety affect PCE and alkoxy functional groups is more effective to increase PCE. Especially, methoxy group increased J_{SC} and 2-ethylhexyloxy group increased V_{OC} . Therefore, for deep study about effects of functional groups on donor moiety, the detailed analysis will be described in 2.4 section.

2.4.1 Light harvesting efficiency

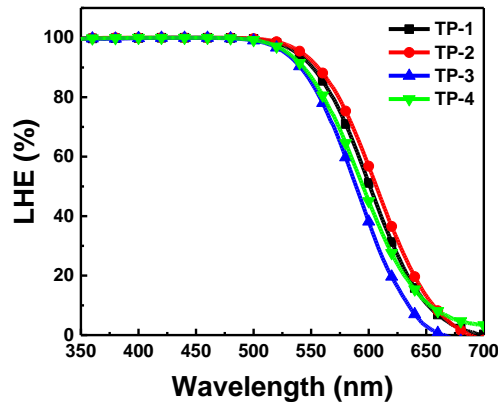


Figure 2.6 LHE of TP-series on thin photoelectrodes.

Light harvesting efficiency (η_{lh} , LHE) plays a critical role to determine PCE on thin TiO₂ films. Therefore, LHE is directly related PCE because all TP-series devices were fabricated with thin TiO₂ film. The LHE equation is described by⁴

$$LHE = 1 - 10^{-A} \quad \text{equation (3)}$$

A is the absorbance of the dyes adsorbed on thin TiO₂ film (Figure 2.3b). When the LHE were measured, the result is in the order of TP-2, TP-1, TP-4 and TP-3. Although the tendency of PCE is not in a good agreement with LHE exactly because of low charge injection efficiency and charge regeneration yield of TP-1, overall tendency of LHE corresponds with the tendency of PCE. Namely, functional groups affect LHE and methoxy group is the most favorable to LHE.

2.4.2 Charge injection efficiency

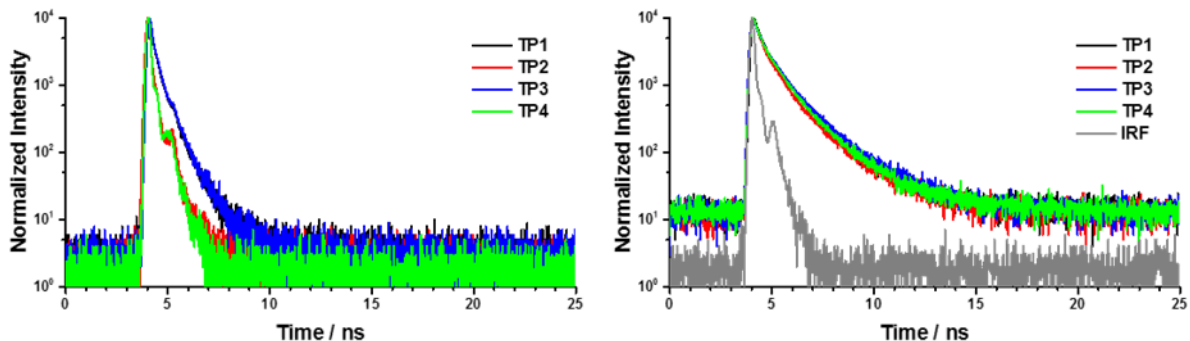


Figure 2.7 Time-correlated single photon counting (TCSPC) of TP-series (a) on TiO₂ 1.8 μm layer and (b) on ZrO₂ films : 448.4 nm excitation and 689.4 nm detection.

Charge injection efficiency (η_{inj}) is calculated by the equation (3)

$$\eta_{inj} = 1 - \tau_{inj}/\tau_{inert} \quad \text{equation (4)}$$

τ_{inj} is the injection life-time which is exciton life-time of dyes on TiO₂ film and τ_{inert} is the inert life-time of excited electrons of dyes measured on ZrO₂ film. When dyes are excited on TiO₂ film, the excited electrons of dyes are transferred to TiO₂ conduction band. Therefore, shorter life-time indicate the better injection ability of dyes. On the other hands, life-times measured on ZrO₂ film indicate self-quenching of dyes because excited electrons can't be injected to conduction band of ZrO₂ which is higher than LUMO of dyes. Both τ_{inj} and τ_{inert} were measured by time-correlated single-photon counting (TCSPC) and are shown in Figure 2.7 and the values are shown in Table 2.3. In the case of the inert life-time measurement on the ZrO₂ film, the TP-series have similar τ_{inert} values, whereas the τ_{inj} values of TP-series measured on TiO₂ films shows significant difference. TP-2 and TP-4 with alkoxy groups exhibit shorter τ_{inj} values of 14.9 ps and 17.3 ps than TP-1 and TP-3 values of 42.0 ps and 36.1 ps. To use this equation (4), η_{inj} of TP-series are calculated to be 0.892, 0.960, 0.912 and 0.957 respectively. In conclusion of this result, TP-2 and TP-4 have better injection efficiency than TP-1 and TP-3. This is because the alkoxy group of TP-2 and TP-4 showed a strong electron donating effect, which significantly increased the injection efficiency. However, TP-3 showed relatively low η_{inj} because carbazole did not act as a good donating group as shown in electrophysical properties. From the above results, the injection efficiency (η_{inj}) is influenced by the presence or absence of the functional group on the donor and depends on electron donating contribution of functional groups on a donor.

Dye	τ_{inj} (ps)	τ_{inert} (ps)	η_{inj}
TP-1	42.0	387.8	0.892
TP-2	14.9	375.2	0.960
TP-3	36.1	411.7	0.912
TP-4	17.3	404.1	0.957

Table 2.3 τ_{inj} on TiO₂ and τ_{inj} on ZrO₂ by Time-Correlated Single Photon Counting (TCSPC) of TP-series

2.4.3 Charge regeneration efficiency

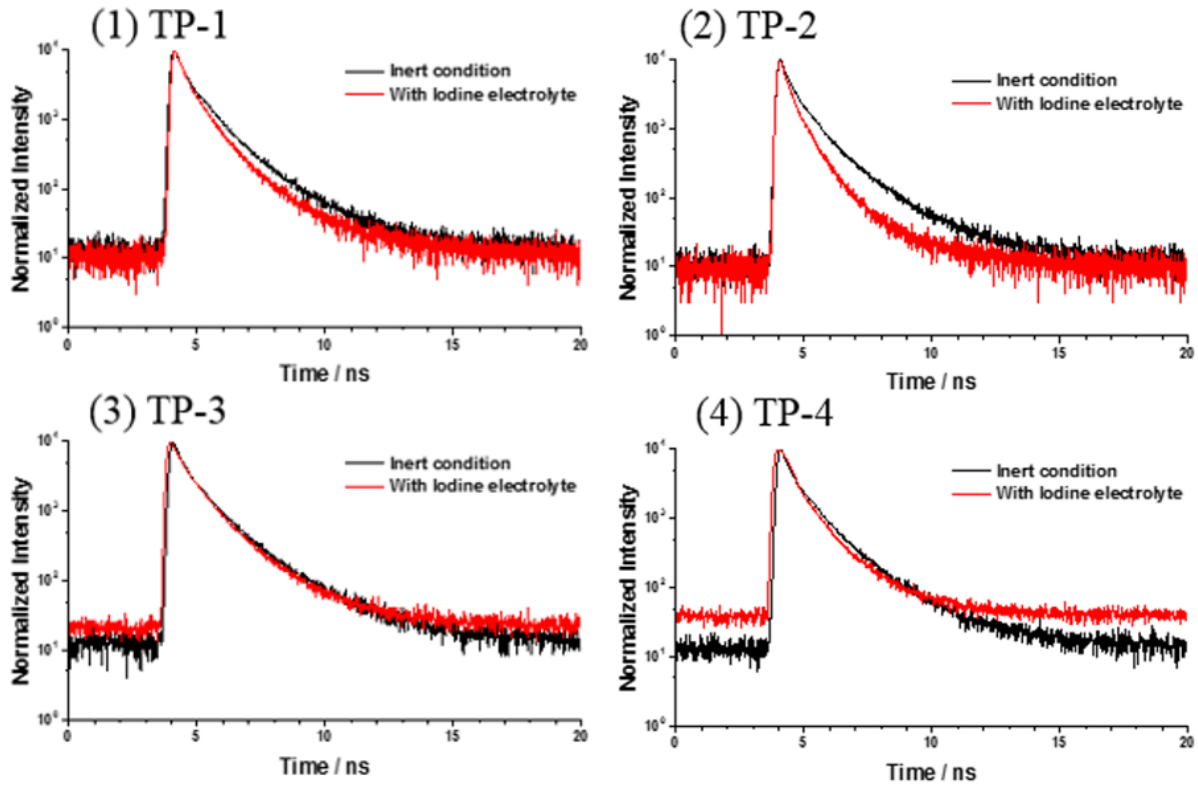


Figure 2.8 Time-correlated single photon counting (TCSPC) of TP-series with iodine electrolyte and without electrolyte.

Charge regeneration efficiency (η_{reg}) exhibits how well oxidized dyes are regenerated from the redox shuttles in electrolyte. The charge regeneration efficiency could be measured by time-correlated single photon counting (TCSPC). For measuring η_{reg} , two types of dummy cells were fabricated with I_3^-/I^- electrolyte and without I_3^-/I^- electrolyte (inert electrolyte) and both types were composed of ZnO_2 semiconductor not TiO_2 semiconductor for preventing injection of excited electrons to semiconductor by light source. In case of dummy cells with I_3^-/I^- electrolyte, excited dyes are regenerated from the I_3^-/I^- redox shuttles. Therefore, short exciton life-time with I_3^-/I^- electrolyte means dye have fast regeneration from the I_3^-/I^- . On the other hands, in the inert cases, excited dyes was quenched naturally without regeneration. Considering the two things, η_{reg} is calculated by

$$\eta_{\text{reg}} = 1 - \tau_{\text{reg}}/\tau_{\text{inert}}, \quad \text{equation (5)}$$

τ_{reg} is the exciton lifetime with iodine electrolyte and τ_{inert} is the exciton lifetime with inert electrolyte. TP-series were excited by 448.4 nm laser and the PL signal was detected at 689.4 nm wavelength. The

rates of PL quenching on TP-series were shown in Figure 2.8, and summarized at Table 2.4. τ_{reg} of TP-series were 114.0 ps, 57.4 ps, 163.9 ps and 96.3 ps respectively. Therefore, the order in which the regeneration efficiency (η_{reg}) increases is as follows : TP-2 (0.850) < TP-4 (0.761) < TP-1 (0.708) < TP-3 (0.602). This result corresponds with J_{SC} tendency of TP-series because nonbonding electrons on methoxy groups of TP-2 attract iodine strongly. Therefore, by the same principle, the location of the attracted iodine by alkoxy group is good at regenerating oxidized TP-2 and TP-4 efficiently. On the other hands, carbazole groups of TP-3 not only have no effect to attract iodide ions (redox mediators) but also shield the HOMO of TP-3, triphenylamine part, from the iodide ions. As we mentioned above, carbazole groups were not part of the HOMO so TP3 showed the lowest τ_{reg} . As a result, TP-2 has the best regeneration efficiency due to methoxy groups and TP-3 has the worst regeneration efficiency due to HOMO screening of carbazole groups. However, this attracting effect of TP-2 is applied to charge recombination. This recombination problem will be treated at V_{OC} section.

Dye	τ_{reg} (ps)	τ_{inert} (ps)	η_{reg}
TP-1	114.0	387.8	0.708
TP-2	57.4	375.2	0.850
TP-3	163.9	411.7	0.602
TP-4	96.4	404.1	0.761

Table 2.4 Time-Correlated Single Photon Counting (TCSPC) of TP-series on ZrO_2 with iodine electrolyte and without iodine electrolyte.

2.4.4 Charge collection efficiency

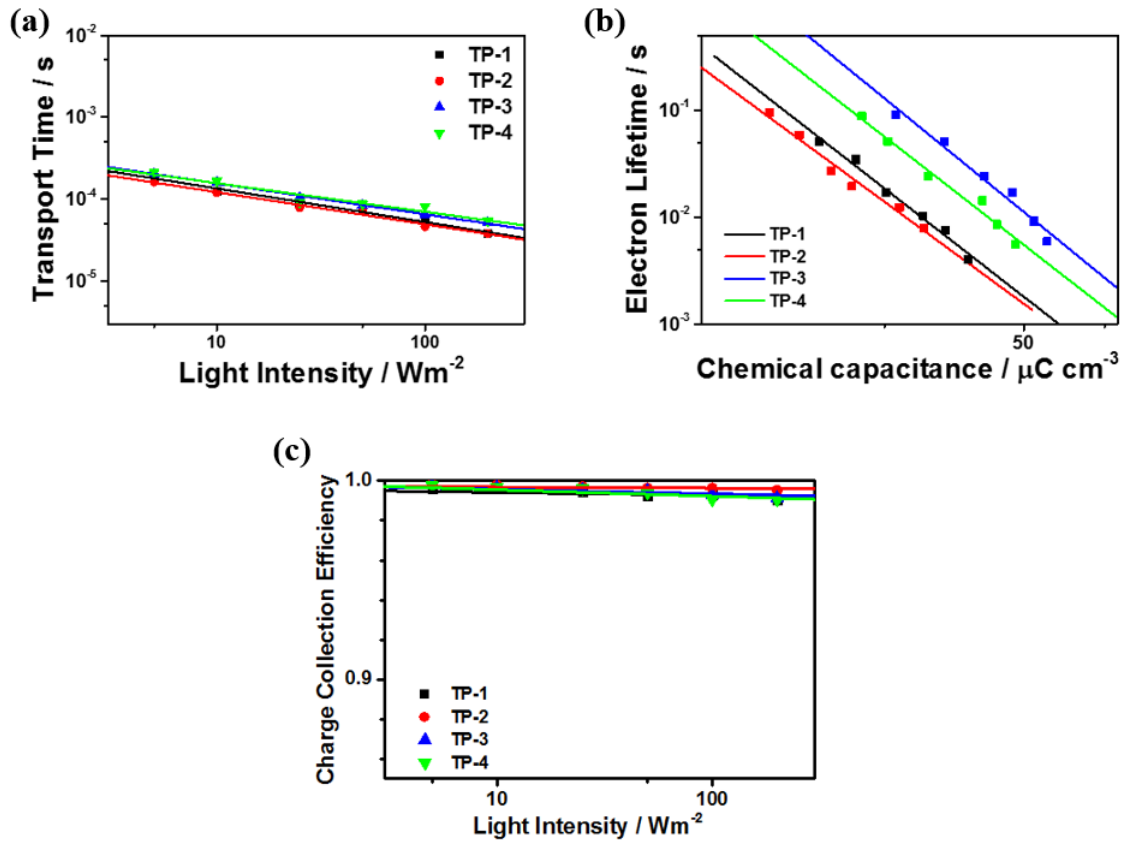


Figure 2.9 (a) Transport times of TP series and (b) electron life-time according to light intensity by IMPS and IMVS. (c) Charge collection efficiency calculated by transport time and electron life-time.

Charge collection efficiency (η_{collect}) is calculated by

$$\eta_{\text{collect}} = 1 - \tau_d / \tau_{\text{rec}} \quad \text{equation (6)}$$

where τ_d is the charge transport time and τ_{rec} is the charge recombination time. These τ_d and τ_{rec} could be obtained by performing intensity modulated photocurrent spectroscopy (IMPS) and intensity modulated photovoltage spectroscopy (IMVS). Figure 2.9 shows IMPS, IMVS and the charge collection efficiency (η_{collect}) of TP series by these two parameters. In Figure 2.9a, there are no significant differences between τ_d of TP-series but in figure 2.9b, τ_{rec} of TP-series show small differences in the order of TP-3 > TP-4 > TP-1 > TP-2. However, these differences are no meaningful because when equation 6 was applied to calculate η_{collect} , all of η_{collect} were over 99% in all intensity. In other words, all of the TP-series have no problems with charge collection efficiency and the reason is due to the planar structures of TP series not functional groups on donor moieties.

2.4.5 Electrochemical impedance spectroscopy (EIS) analysis

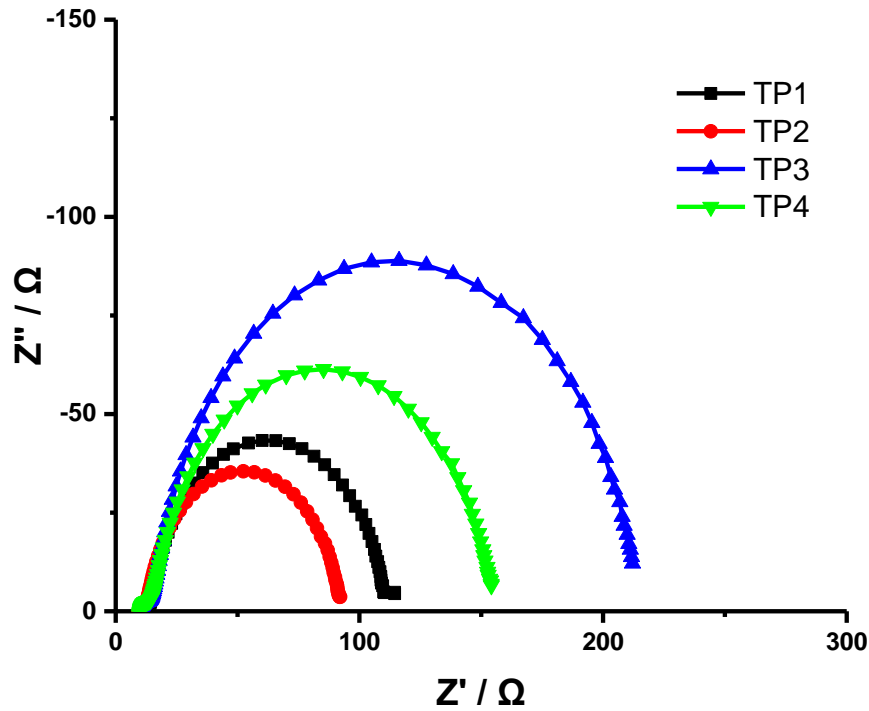


Figure 2.10 Nyquist plot of TP-series measured by electrochemical impedance spectroscopy (EIS) under the dark condition.

EIS have been measured to investigate internal impedance in DSCs and Nyquist plot typically shows three semicircles. At the high-frequency, charge transfer resistance (R_{ct}) at the counter electrode interface indicates. Intermediate semicircle indicates dark reaction impedance (R_d) between TiO_2 /dye/electrolyte interfaces and at the low-frequency, diffusion impedance (R_d) indicates in the electrolyte.⁴⁵ However, Nyquist plot of TP-series shows intermediate semicircle definitely, so charge transfer at counter electrode and diffusion can be ignored. By the intermediate semicircle, recombination order is $TP-3 < TP-4 < TP-1 < TP-2$. The recombination tendency is because carbazole groups of TP-3 interrupt I_3^-/I^- not to approach TiO_2 surface, while oxygen on methoxy groups of TP-2 attract I_3^-/I^- close to TiO_2 surface due to non-pair electron of oxygen. However, recombination was improved by replacing methyl group of methoxy with 2-ethylhexyl group and TP-4 showed decreased charge recombination. In this reason, TP-4 can achieve high V_{oc} .

2.5 Stability test

As DSCs is a study showing the possibility of commercialization like BIPV, it is important to overcome the stress to external environment and to have long life of devices. In this paper, stability tests were conducted on all three natural factors (thermal/light/water).

2.5.1 Thermal stability

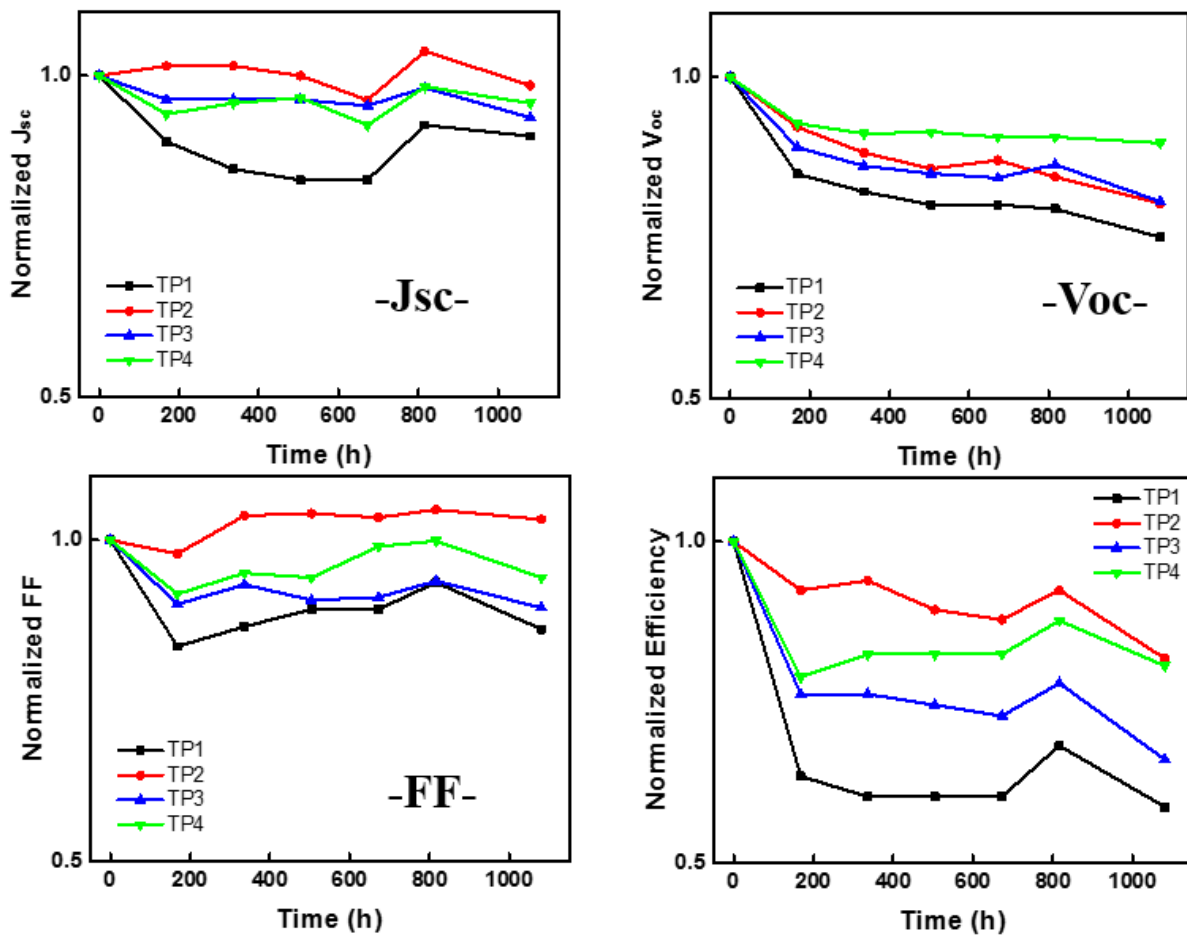


Figure 2.11 The photovoltaic parameters of TP-series with ionic liquid electrolyte at 70°C under dark condition.

Thermal tests were conducted at 70°C under dark condition for 6 weeks. Hence, ionic liquid electrolyte was selected as an electrolyte to avoid volatilization of an electrolyte. The normalized PCE, J_{sc} and V_{oc} of TP-series under thermal stress are shown in Figure 2.11. The initial efficiencies of the

TP-series cells were 6.0%, 6.6%, 5.9%, and 5.9%, respectively, which decreased to 3.5%, 5.4%, 3.9%, and 4.8% after 1080 hours. The efficiency was decreased by 41.2% for, TP-1, 18.2% for TP2, 33.9% for TP3, and 19.3% for TP-4. Critical declines of PCE indicate within about 168 hours which is due to the reduction of the voltage not the current. However after initial 168 hours, there were not big change of PCE showing stable efficiency. As a result, the reduction of the efficiency due to thermal stress is not caused by the damage of the dye because there were no change of PCE since initial decrease of V_{OC} . If dyes were degraded, the PCE must be continuously decreased and reach to 0% of PCE. We concluded interface between electrolyte and the TiO_2 caused decline of PCE so EIS analysis will be conducted in order to analyze relation between V_{OC} and electrolyte from thermal stress.

In particular, TP-3 showed low thermal stability because 3,6-position of carbazole can be easily damaged by thermal stress.⁴⁶⁻⁴⁷ Therefore, 3,6-position of carbazole need to be protected by connecting alkyl chain at these position to increase the thermal stability.

2.5.2 Light stability

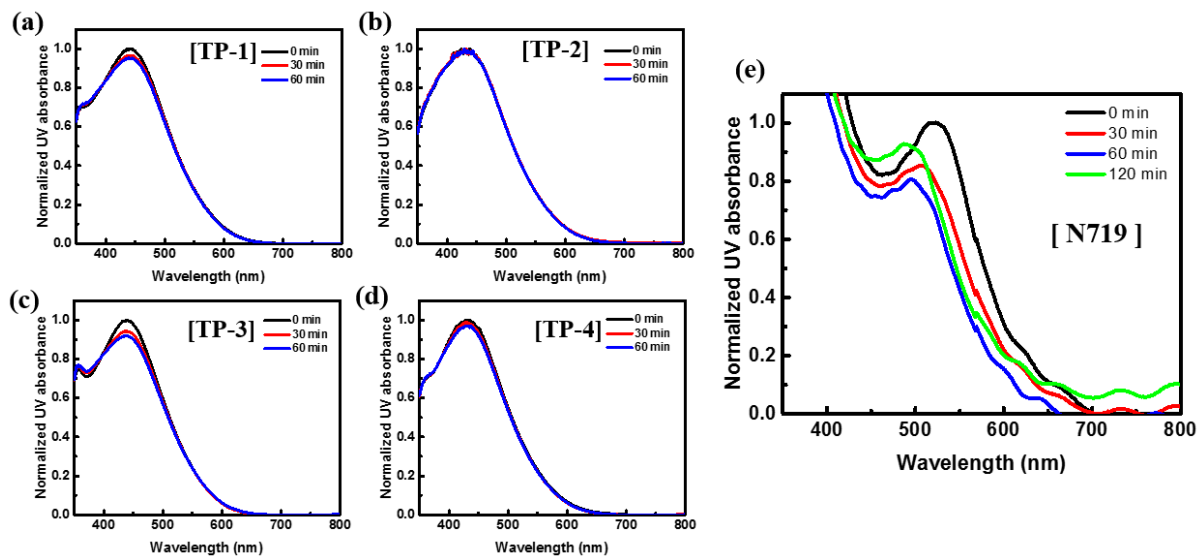


Figure 2.12 Normalized UV absorbance of (a) TP-1, (b) TP-2, (c) TP-3, (d) TP-4 and (e) N719 on TiO_2 film according to light soaking time.

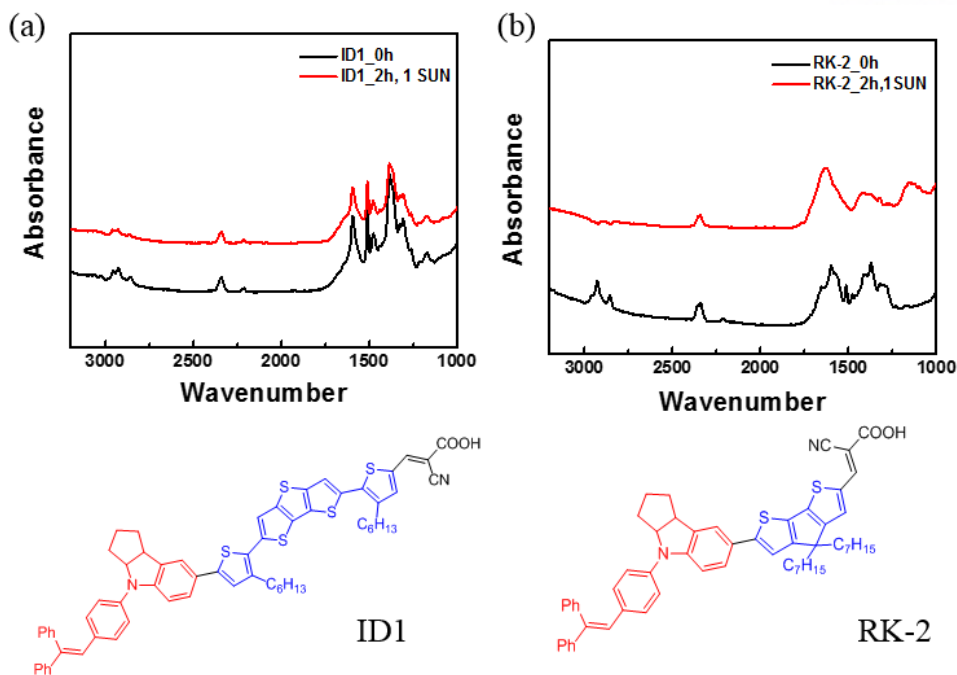


Figure 2.13 FT-IR spectra of ID1 and RK-2 after 2 hours 1 SUN light soaking.

Light stability of TP-series was investigated by UV spectroscopy according to the light soaking time and the data were shown in Figure 2.13. TP-3 showed relatively low light stability while, TP-2 showed strong light stability because 3,6-position of carbazole can be also damaged easily by light. However, there is no position where TP-2 was attacked by light. Therefore, TP-4 also showed relatively high light stability.

In these results, all of the TP-series exhibit strong light stability without big change of the UV absorbance contrary to the N719 data (e). In order to know the reason TP-series have good light stability, we hypothesized that π -bridge like a dithieno[3,2-*b*:2',3'-*d*]thiophene (DTT) is critical factor making TP-series light stable because frameworks of TP-series are the same except functional groups on donor moiety. To demonstrate the effect of dithieno[3,2-*b*:2',3'-*d*]thiophene (DTT) directly, I synthesized DTT based ID1 dye and cyclopentadithiophene based RK-2 dye and they were measured by FT-IR after 1 SUN light ageing. In Figure 2.13, ID1 dye and RK-2 dye showed FT-IR spectra after the 2 hours 1 SUN light ageing. In case of ID1 dye, there were no change of absorbance shape but RK-2 showed absorbance shape get shapeless. It is the demonstration that dithieno[3,2-*b*:2',3'-*d*]thiophene (DTT) have strong light stability and cyclopentadithiophene was damaged by light because two dyes have same structure except π -bridge units. In this way, we demonstrated that π -conjugated framework is vital to determine light stability. In summary, functional groups affect the light stability slightly but rigidity of framework is critical to determine the light stability.

2.5.3 Water stability

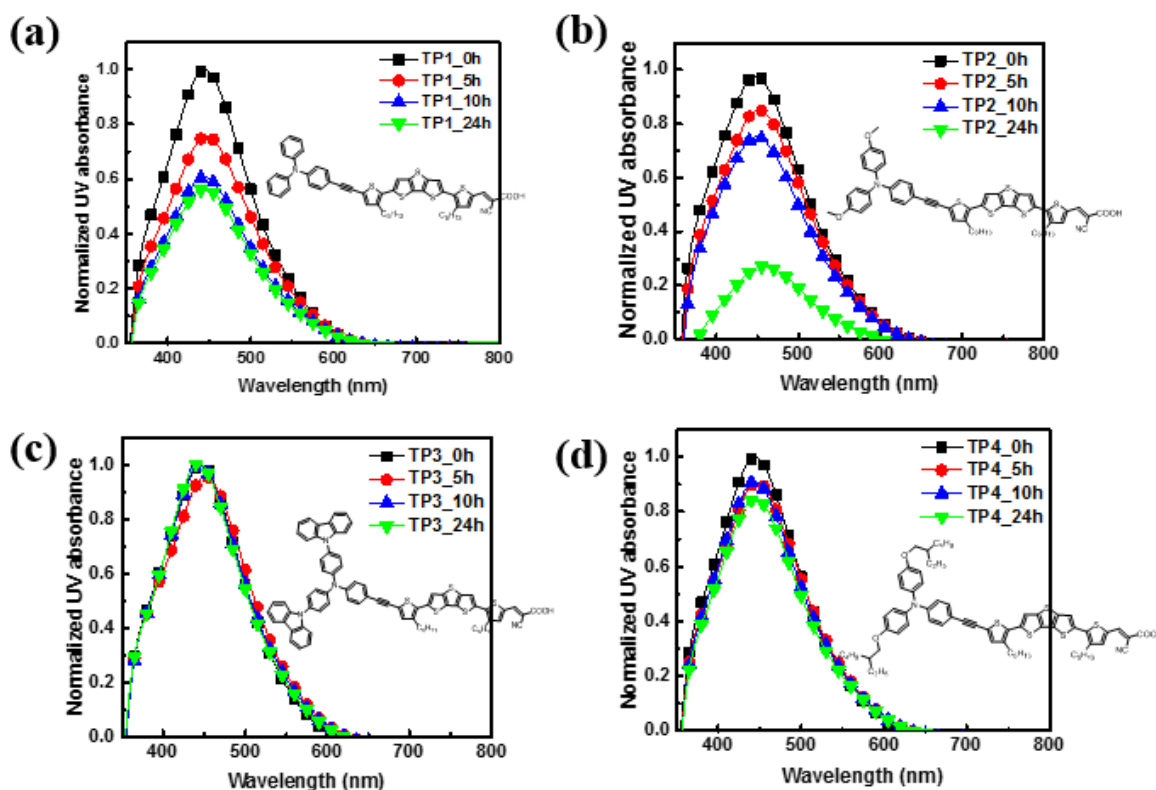


Figure 2.14 Normalized UV absorbance of (a) TP-1, (b) TP-2, (c) TP-3 and (d) TP-4 on TiO₂ film according to submersion time.

To evaluate the stability of TP-series in water, UV spectroscopy of the dye adsorbed TiO₂ films were measured according to immersion time in a solution of acetonitrile and water in a ratio of 9:1. The dye adsorbed TiO₂ film was also checked by UV absorption at 1 hour, 5 hours, 10 hours and 24 hours intervals. Since the solution contained 10% water, it is possible to expect a change in the long time of general humidity condition even with a short time measurements. Figure 2.14 shows the normalized film UV data of TP-series according to immersion time. These data exhibit that the intensities of absorbance are lowered depending on the immersion time in the solution. Among them, TP-3 shows the most stable absorption state on TiO₂ film without the change of intensity. On the other hands, TP-2 was severely desorbed from TiO₂ film depending on the immersion time, and all of TP-2 dyes were almost desorbed after 24 hours. Considering these results and the previous water stability research that water molecules react with anchoring groups between dye and TiO₂, characteristics of the functional groups on donor moiety is critical to water stability.⁴⁸ In case of carbazole in TP-3, water molecules did not approach the anchoring groups by very strong hydrophobic properties of carbazoles. On the contrary,

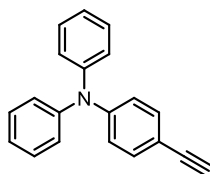
methoxy groups attract water molecules due to the hydrogen bonds between water and methoxy group allowing water molecules to reach the anchoring group. In order to solve the problem of low water stability of TP-2, we introduced 2-ethylhexyloxy group in place of methoxy group to interfere with hydrogen bonding between oxygen in functional group and water molecules. The newly designed dye, TP-4, actually exhibits the improved water stability. As a result, these water stability tests demonstrate correlation between the properties of functional groups on donor and water stability.

III. Experimental method

3.1 Synthesis : TP-series dyes and Bestmann-reagent

All chemicals and reagents were purchased from Aldrich, Alfa Aesar, Matrix Scientific and TCI without further purification. All reactions were performed with anhydrous solvent prepared by molecular sieves prior to use and nitrogen atmosphere unless otherwise noted.

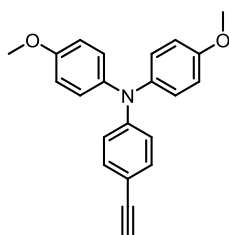
The synthesis of the intermediates 1-4, 5-6, 8 and 10 were carried out as previously reported.



4-ethynyl-N,N-diphenylaniline (D-1)

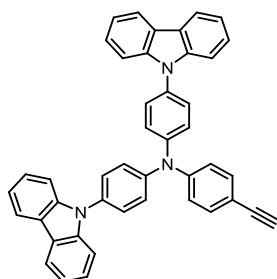
To a mixture of **compound 5** (3 g, 10.97 mmol) and K_2CO_3 (3 g, 22.00 mmol) in anhydrous THF/MeOH (1:1 = 25 ml : 25 ml), Bestmann-Ohira reagent (2.5 mg, 13.17 mmol) was added at room temperature. The solution was stirred at room temperature for overnight. The crude mixture was filtered through a celite (dichloromethane was used for solvent). The residue was extracted with dichloromethane and 5% $NaHCO_3$ (aq). The organic solvent was removed reduced pressure and purified by column chromatography with Hex/EA (7:1) as a white solid (1.91 g, 64.7%). 1H NMR (400 MHz, $CDCl_3$) δ (ppm): δ 3.04 (s, 1H), 6.99 (m, 2H), 7.09 (d, $J=1.1$ Hz, 1H), 7.10-7.14 (m, 5H), 7.28–7.27 (m, 1H), 7.30 (d, $J=1.1$ Hz, 2H), 7.31-7.32 (m, 1H), 7.34-7.32 (m, 2H); ^{13}C NMR (100 MHz, $CDCl_3$) : δ 76.14, 83.90, 114.73, 122.03, 123.61, 125.02, 129.38, 133.03, 147.10, 148.33; HRMS (EI) : Exact mass Calcd. for $C_{20}H_{15}N$ $[M]^+$: 269.1204, found 269.1204.

Synthetic methods of **Compound D-2, D-3 and D-4** are the same as that of **D-1**.



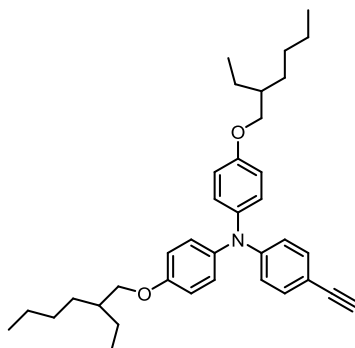
4-ethynyl-N,N-bis(4-methoxyphenyl)aniline (D-2)

Compound 7 (0.62 g, 1.86 mmol), K_2CO_3 (0.514 g, 3.72 mmol) and Bestmann-Ohira reagent (0.71 g, 3.72 mmol) were used in anhydrous THF/MeOH (1:1 = 10 ml : 10 ml). A sticky yellow liquid was obtained (0.218 g, 35.6%). 1H NMR (400 MHz, $CDCl_3$) δ (ppm): δ 2.99 (s, 1H), 3.80 (s, 6H), 6.81 (d, $J=8.8$ Hz, 2H), 6.84 (d, $J=8.8$ Hz, 4H), 7.06 (d, $J=8.8$ Hz, 4H), 7.27 (d, $J=8.8$ Hz, 2H); ^{13}C NMR (100 MHz, $CDCl_3$) : δ 55.50, 75.63, 76.76, 114.85, 118.93, 127.18, 132.95, 140.12, 156.39



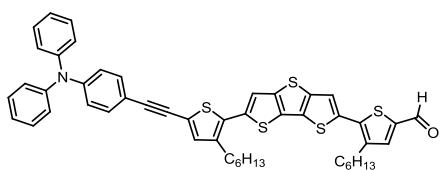
N,N-bis(4-(9H-carbazol-9-yl)phenyl)-4-ethynylaniline (D-3)

Compound 9 (370 mg, 1.35 mmol), K_2CO_3 (373 mg, 2.70 mmol) and Best-mann reagent (312 mg, 1.624 mmol) were used in anhydrous THF/MeOH (1:1 = 10 ml : 10 ml). A sticky white liquid was obtained (202 mg, 25%). 1H NMR (400 MHz, $CDCl_3$) δ (ppm): δ 3.12 (s, 1H), 7.34 (m, 4H), 7.49 (m, 20H), 8.19 (d, $J=7.1$ Hz, 4H).



4-((2-ethylhexyl)oxy)-N-(4-((2-ethylhexyl)oxy)phenyl)-N-(4-ethynylphenyl)aniline (D-4)

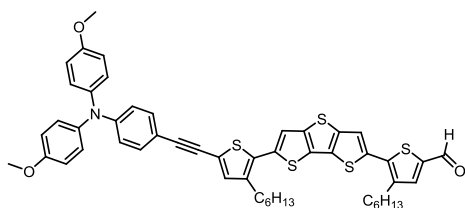
Compound 11 (1.04 g, 1.96 mmol), K₂CO₃ (540 mg, 3.92 mmol) and Best-mann reagent (450 mg, 2.35 mmol) were used in anhydrous THF/MeOH (1:1 = 15 ml : 15 ml). A sticky white liquid was obtained (202 mg, 20%). ¹H NMR (400 MHz, CDCl₃) δ (ppm): δ 0.91 (m, 12H), 1.32 (m, 8H), 1.46 (m, 8H), 1.71 (m, 2H), 6.80 (d, *J*=8.9 Hz, 2H), 6.83 (d, *J*=9.0 Hz, 4H), 7.05 (d, *J*=9.0 Hz, 4H), 7.25 (d, *J*=8.0 Hz, 2H); ¹³C NMR (100 MHz, CDCl₃) : δ 11.60, 14.12, 23.08, 23.88, 29.12, 30.56, 39.46, 70.71, 75.47, 84.33, 112.30, 115.37, 118.73, 127.17, 132.89, 139.89, 139.81, 149.32, 156.24.



5-(6-(5-((4-(diphenylamino)phenyl)ethynyl)-3-hexylthiophen-2-yl)dithieno[3,2-b:2',3'-d]thiophen-2-yl)-4-hexylthiophene-2-carbaldehyde (EF-1)

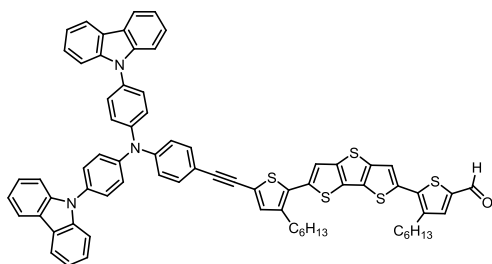
Pd(PPh₃)Cl₂ (10 mg, 0.0149 mmol), CuI (3 mg, 0.0149 mmol), **compound D-1** (86.4 mg, 0.164 mmol) and **compound 4** (95 mg, 0.149 mmol) were suspended under argon to a completely dried and degassed two neck round flask. Degassed solvent (TEA : THF = 3 ml : 9 ml) was injected into the flask and then the mixture was stirred and heated under reflux (65 °C) overnight. After cooling down by room temperature, water (20 ml) was poured slowly and extracted with chloroform. The organic phase was evaporated under reduced pressure and purified by column chromatography with Hex/DCM/EA (3:1:0.1) as a red solid (73 mg, 55%). ¹H NMR (400 MHz, CDCl₃) δ (ppm): δ 0.91 (br t, 6H), 1.32-1.37 (m, 8H), 1.41 (dt, *J*=7.0, 5.4 Hz, 4H), 1.69 (dt, *J*=15.5, 7.8 Hz, 4H), 2.77 (t, *J*=7.6, 2H), 2.84 (t, *J*=8.0, 2H), 7.01 (d, *J*=8.7 Hz, 2H), 7.08 (m, 3H), 7.13 (d, *J*=7.6 Hz, 4H), 7.27-7.30 (m, 4H), 7.31 (d, *J*=1.8 Hz, 1H), 7.35 (d, *J*=8.7 Hz, 2H), 7.43 (s, 1H), 7.59 (s, 1H), 9.82 (s, 1H); ¹³C NMR (100 MHz, CDCl₃-d₆) : δ 14.1, 22.6, 29.2, 29.4, 29.5, 30.3, 30.4, 31.7, 14.1, 81.8, 95.0, 115.3, 119.1, 120.6, 122.0, 122.4, 123.7, 125.1, 129.4, 131.6, 131.9, 132.4, 134.5, 135.4, 137.3, 138.9, 140.2, 140.6, 140.7, 141.0, 142.3, 147.1, 148.1, 182.37; HRMS (EI) : Exact mass calcd. for C₄₉H₄₅NOS₅ [M]⁺ : 823.2105, found 823.2105.

Synthetic methods of **Compound EF-2**, **EF-3** and **EF-4** are the same as that of **Compound EF-1**.



5-(6-(5-((4-(bis(4-methoxyphenyl)amino)phenyl)ethynyl)-3-hexylthiophen-2-yl)dithieno[3,2-b:2',3'-d]thiophen-2-yl)-4-hexylthiophene-2-carbaldehyde (EF-2)

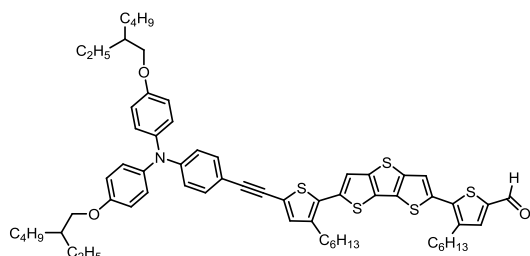
Pd(PPh₃)Cl₂ (20 mg, 0.028 mmol), CuI (7 mg, 0.037 mmol), **Compound D-2** (94.2 mg, 0.286 mmol) and **compound 4** (200 mg, 0.314 mmol) were suspended under argon to a completely dried and degassed two neck round flask. Degassed solvent (TEA : THF = 6 ml : 18 ml) was injected into the flask. The orange solid was obtained (209 mg, 83%). ¹H NMR (400 MHz, CDCl₃) δ (ppm): δ 0.90 (br m, 6H), 1.32 (m, 8H), 1.41 (br m, 4H), 1.68 (br m, 4H), 2.78 (t, *J*=7.6, 2H), 2.86 (t, *J*=8.0, 2H), 3.81 (s, 6H), 6.86 (m, 5H), 7.08 (m, 5H), 7.26 (d, *J*=8.4 Hz, 1H), 7.28 (d, *J*=8.4 Hz, 2H), 7.31 (s, 1H), 7.47 (s, 1H), 7.62 (s, 1H), 9.85 (s, 1H); ¹³C NMR (100 MHz, DMSO-d₆/CDCl₃ (v/v=1/1)) : δ 13.68, 21.94, 28.48, 28.63, 29.47, 29.73, 30.96, 54.91, 80.66, 95.07, 111.75, 114.54, 117.63, 119.13, 120.51, 121.57, 126.97, 129.40, 130.78, 131.69, 133.47, 133.92, 134.78, 136.18, 138.95, 139.72, 140.01, 141.54, 142.07, 148.65, 156.07; HRMS (FAB⁺) : Exact mass calcd for C₅₁H₄₉NO₃S₅ [M]⁺: 883.2316, found 883.2318.



5-(6-(5-((4-(bis(4-(9H-carbazol-9-yl)phenyl)amino)phenyl)ethynyl)-3-hexylthiophen-2-yl)dithieno[3,2-b:2',3'-d]thiophen-2-yl)-4-hexylthiophene-2-carbaldehyde (EF-3)

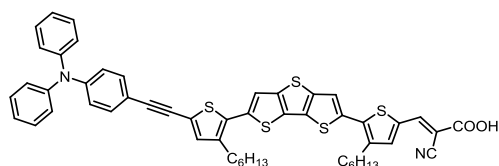
Pd(PPh₃)Cl₂ (5 mg, 0.007 mmol), CuI (3 mg, 0.016 mmol), **Compound D-3** (46.2 mg, 0.077 mmol) and **compound 4** (48.9 mg, 0.077 mmol) were suspended under argon to a completely dried and degassed two neck round flask. Degassed solvent (TEA : THF = 3 ml : 9 ml) was injected into the flask. The orange solid was obtained (30 mg, 34%). ¹H NMR (400 MHz, CDCl₃) δ (ppm): δ 0.90 (br m, 6H), 1.33 (m, 8H), 1.42 (br m, 4H), 1.69 (br m, 4H), 2.80 (t, *J*=8.0, 2H), 2.86 (t, *J*=7.6, 2H), 7.15 (s, 1H), 7.29 (d, *J*=3.2 Hz, 2H), 7.31 (s, 2H), 7.33 (s, 1H), 7.34 (s, 1H), 7.43-7.56 (m, 20H), 7.63 (s, 1H), 8.16

(d, $J=7.6$ Hz, 4H), 9.85 (s, 1H); HRMS (FAB⁺) : Exact mass calcd for C₇₃H₅₉N₃OS₅ [M]⁺: 1153.3262, found 1154.3350.



5-(6-(5-((4-(bis(4-((2-ethylhexyl)oxy)phenyl)amino)phenyl)ethynyl)-3-hexylthiophen-2-yl)dithieno[3,2-b:2',3'-d]thiophen-2-yl)-4-hexylthiophene-2-carbaldehyde (EF-4)

Pd(PPh₃)Cl₂ (10 mg, 0.015 mmol), CuI (3 mg, 0.015 mmol), **Compound D-4** (86.4 mg, 0.164 mmol) and **compound 4** (95 mg, 0.149 mmol) were suspended under argon to a completely dried and degassed two neck round flask. Degassed solvent (TEA : THF = 3 ml : 9 ml) was injected into the flask. The orange solid was obtained (50 mg, 31%).

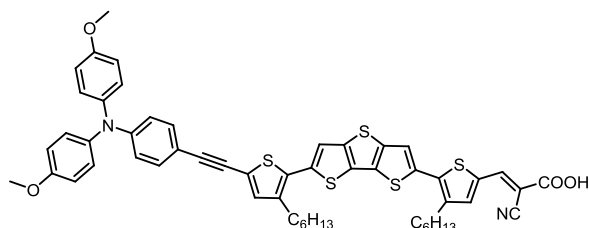


(E)-2-cyano-3-(5-(6-(5-((4-(diphenylamino)phenyl)ethynyl)-3-hexylthiophen-2-yl)dithieno[3,2-b:2',3'-d]thiophen-2-yl)-4-hexylthiophen-2-yl)acrylic acid (TP-1)

Compound EF-1 (55 mg, 0.046 mmol) and cyanoacetic acid (15 mg, 0.185 mmol) were suspended into a 150 ml flask. Solvent (chloroform : Acetonitrile = 12 ml : 4 ml) was injected into the flask and piperidine (15 mg, 0.185 mmol) was added slowly. The mixture was heated at reflux (60~70°C) overnight. When the reaction was completed, water was poured at room temperature to quench the reaction. The mixture product was extracted with chloroform and washed with brine. The organic layer was evaporated under reduced pressure and purified with column chromatography with MC first and MC:MeOH:AcOH mixture solvent (v/v/v=10:1:0.1) finally as a reddish black solid (60 mg, 99%). ¹H NMR (400 MHz, DMSO-d₆/CDCl₃ (v/v=1:1)) δ (ppm): δ 0.83 (br m, 6H), 1.31 (br m, 12H), 1.63 (br m, 4H), 2.74 (t, $J=7.6$ Hz, 2H), 2.81 (t, $J=7.6$, 2H), 6.90 (d, $J=8.4$, 2H), 7.04 (m, 5H), 7.09 (s, 1H), 7.27 (m, 6H), 7.42 (s, 1H), 7.62 (s, 1H), 7.67 (s, 1H), 7.69 (s, 1H), 8.24 (s, 1H); ¹³C NMR (100 MHz, DMSO-d₆/CDCl₃ (v/v=1/1)) : δ 14.2, 22.5, 29.0, 29.1, 29.2, 30.1, 30.3, 31.5, 81.8, 95.1, 114.8, 117.5, 119.8, 121.0, 121.6, 121.9, 124.1, 125.2, 129.7, 130.1, 131.3, 131.6, 132.4, 134.3, 134.8, 135.5, 136.6, 139.9,

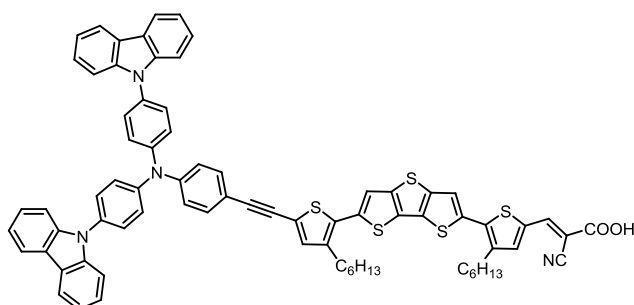
140.6, 142.1, 142.5, 143.8, 146.8, 148.2, 164.5; HRMS (ESI) : Exact mass calcd for C₅₂H₄₆N₂O₂S₅ [M]⁺: 890.2163, found 890.2158.

Synthetic methods of **TP-2**, **TP-3** and **TP-4** are the same as that of **TP-1**.



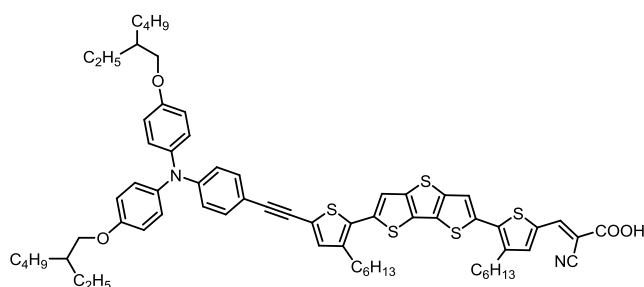
(E)-3-(5-(6-(5-((4-(bis(4-methoxyphenyl)amino)phenyl)ethynyl)-3-hexylthiophen-2-yl)dithieno[3,2-b:2',3'-d]thiophen-2-yl)-4-hexylthiophen-2-yl)-2-cyanoacrylic acid (TP-2)

Compound EF-2 (209 mg, 0.236 mmol) and cyanoacetic acid (80 mg, 0.945 mmol) were suspended into a 150 ml flask. Solvent (chloroform : Acetonitrile = 21 ml : 7 ml) was injected into the flask and piperidine (80 mg, 0.945 mmol) was added slowly. The mixture was heated at reflux (60~70°C) overnight. A reddish black solid was gained (100 mg, 44 %). ¹H NMR (400 MHz, DMSO-d₆/CDCl₃ (v/v=1/1)) δ (ppm) : δ 0.82 (br m, 6H), 1.25 (br m, 10H), 1.60 (d, 5H), 2.75 (m, 5H), 3.73 (s, 6H), 6.64 (d, *J*=8.7 Hz, 2H), 6.95–6.91 (m, 4H), 7.11–7.06 (m, 4H), 7.22 (s, 1H), 7.28 (d, *J*=8.6 Hz, 2 H), 7.82 (d, 7.8 Hz, 1H); ¹³C NMR (100 MHz, DMSO-d₆) : δ 14.2, 22.5, 29.0, 29.1, 29.2, 30.1, 30.3, 31.5, 55.5, 78.9, 81.2, 95.6, 112.4, 115.0, 118.3, 119.6, 121.0, 122.2, 127.5, 130.0, 131.3, 131.4, 132.2, 134.4, 135.3, 136.8, 139.5, 140.3, 140.6, 142.0, 142.6, 149.2, 156.6; HRMS (ESI) : Exact mass calcd for C₅₄H₅₀N₂O₄S₅ [M]⁺: 950.2374, found 950.2375.



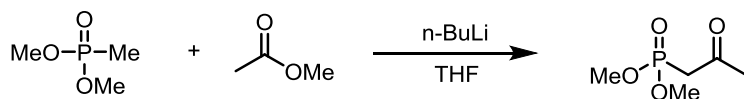
(E)-3-(5-(6-(5-((4-(bis(4-(9H-carbazol-9-yl)phenyl)amino)phenyl)ethynyl)-3-hexylthiophen-2-yl)dithieno[3,2-b:2',3'-d]thiophen-2-yl)-4-hexylthiophen-2-yl)-2-cyanoacrylic acid (TP-3)

Compound EF-3 (69 mg, 0.060 mmol) and cyanoacetic acid (50 mg, 0.597 mmol) were suspended into a 150 ml flask. Solvent (chloroform : Acetonitrile = 15 ml : 5 ml) was injected into the flask and piperidine (50 mg, 0.597 mmol) was added slowly. The mixture was heated at reflux (60~70 °C) overnight. A reddish black solid was gained (58 mg, 79%). ¹H NMR (400 MHz, DMSO-d₆/CDCl₃ (v/v=1/1)) δ (ppm) : δ 0.82 (br m, 6H), 1.27 (br m, 10H), 1.63 (m, 5H), 2.78 (dt, *J*=16.7, 7.7 Hz, 5H), 7.17 (s, 1H), 7.21 (d, *J*=1.1 Hz, 1H), 7.23 (m, 2H), 7.24 (m, 2H), 7.36 (d, *J*=1.3 Hz, 1H), 7.46–7.38 (m, 14H), 7.49 (m, 2H), 7.54 (m, 4H), 7.61 (s, 1H), 7.64 (s, 1H), 8.11 (dt, *J*=7.7, 0.9 Hz, 4H), 8.17 (s, 1H); ¹³C NMR (100 MHz, DMSO-d₆) : δ 14.3, 22.5, 22.6, 24.1, 24.2, 25.4, 26.1, 29.0, 29.2, 30.1, 30.3, 31.5, 82.3, 94.9, 110.0, 116.3, 117.5, 120.0, 120.2, 120.5, 121.1, 121.7, 123.1, 123.2, 126.0, 126.2, 128.2, 130.1, 131.3, (131.8), 131.9, 132.8, 132.9, 134.4, 135.1, 135.5, 136.5, 140.4, 140.6, 140.7, 142.2, 142.6, 145.8, 147.7, 164.3; HRMS (FAB⁺) : Exact mass calcd for C₇₆H₆₀N₄O₂S₅ [M]⁺: 1220.3320, found 1121.3379.



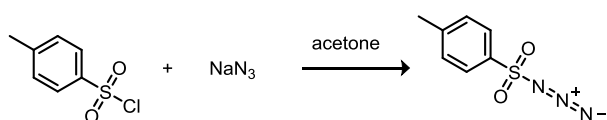
(E)-3-(5-(6-(5-((4-(bis(4-((2-ethylhexyl)oxy)phenyl)amino)phenyl)ethynyl)-3-hexylthiophen-2-yl)dithieno[3,2-b:2',3'-d]thiophen-2-yl)-4-hexylthiophen-2-yl)-2-cyanoacrylic acid (TP-4)

Compound EF-4 (50 mg, 0.046 mmol) and cyanoacetic acid (15 mg, 0.185 mmol) were suspended into a 150 ml flask. Solvent (chloroform : Acetonitrile = 7 ml : 7 ml) was injected into the flask and piperidine (15 mg, 0.185 mmol) was added slowly. The mixture was heated at reflux (60~70 °C) overnight. A reddish black solid was gained (30 mg, 56%). ¹H NMR (400 MHz, DMSO-d₆/CDCl₃ (v/v=1/1)) δ (ppm) : δ 0.93 (br m, 18H), 1.34 (br m, 16H), 1.46 (br m, 12H), 1.70 (br m, 6H), 2.80 (t, *J*=8.0 Hz, 2H), 2.86 (t, *J*=7.7 Hz, 2H), 3.85 (d, *J*=5.7 Hz, 4H), 6.78 (d, *J*=8.8 Hz, 2H), 6.90 (d, *J*=8.9 Hz, 4H), 7.08 (d, *J*=8.9 Hz, 4H), 7.14 (s, 1H), 7.27 (d, *J*=8.7 Hz, 2H), 7.49 (s, 1H), 7.57 (s, 1H), 7.62 (s, 1H), 8.16 (s, 1H); HRMS (FAB⁺) : Exact mass calcd for C₆₈H₇₈N₂O₄S₅ [M]⁺: 1146.4565, found 1146.4563.



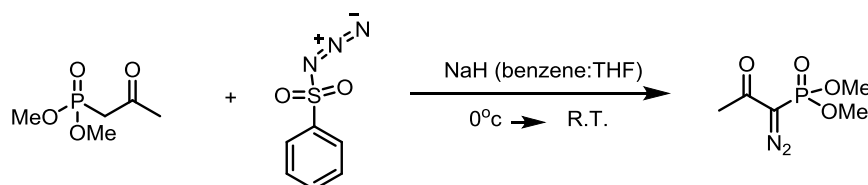
dimethyl (2-oxopropyl)phosphonate⁴⁹

To round bottom flask, magnetic bar was put and creating a vacuum on the inside of the flask. Dimethyl methane phosphonate (10 g, 80 mmol) and THF (80 ml) were injected in the flask and making -78°C condition. After 5 min, 2.5 M n-BuLi (32 ml, 80 mmol) was added drop-wisely and stirring the solution for 30 min. Methyl acetate (13.5 g, 184 mmol) with 10 ml THF was added slowly to the mixture at -78°C continuously. After 1 hour, the temperature of the mixture was raised up to 0°C and then, 1 M HCl solution was added slowly for 5 min. The mixture was extracted with DCM three times, dried with MgSO₄ and filtered. The organic solution was concentrated under reduced pressure below 30°C. The bright yellow and stick liquid was gained (7.8 g, 58.6 %). ¹H NMR (400 MHz, CDCl₃) δ (ppm) : δ 2.25 (s, 1H), (d, *J*=22.7 Hz, 3H), 3.72 (d, *J*=11.2 Hz, 6H).



4-methylbenzenesulfonyl azide⁵⁰

To a round bottom flask, tosyl chloride (10 g, 52 mmol) was added in acetone 100 ml reducing temperature by 0 °C. A sodium azide (5 g, 77 mmol) in water was injected in the flask at 0°C continuously. The solution was be warm up to room temperature and the solution was stirred overnight. The acetone in the mixture was removed under reduced pressure. The mixture was extracted with ether 3 times and the organic layer was dried with MgSO₄. Finally, the ether solvent was removed under reduced pressure. Yellow sticky liquid was gained (9 g, 88 %). ¹H NMR (400 MHz, CDCl₃) δ (ppm) : δ 2.45 (s, 3H), 7.38 (d, *J*=8.0 Hz, 2H), 7.80 (d, *J*=8.4 Hz, 2H).



dimethyl (1-diazo-2-oxopropyl)phosphonate⁴²

NaH (1.5 g, 62 mmol) in anhydrous benzene (80 mL) and anhydrous THF (15mL) was prepared at 0°C. Dimethyl-2-oxopropyl phosphonate (10g, 62mmol) in benzene (25mL) was added to the NaH solution slowly and the mixture was stirred for 1 h at 0°C. 4-methylbenzenesulfonyl azide (12.3 g, 62

mmol) dissolved in benzene (15mL) was injected additionally. The mixture was stirred at room temperature for 2 h and then filtered on celite. The filtered solution was concentrated under reduced pressure. The mixture was purified by short chromatography on silica gel with ethyl acetate and hexane (1:1). The yellow and sticky liquid was gained (6.8 g, 56.6 %). ^1H NMR (400 MHz, CDCl_3) δ (ppm) : 3.85 (d, $J=12.0$ Hz, 6H), 2.26 (s, 3H).

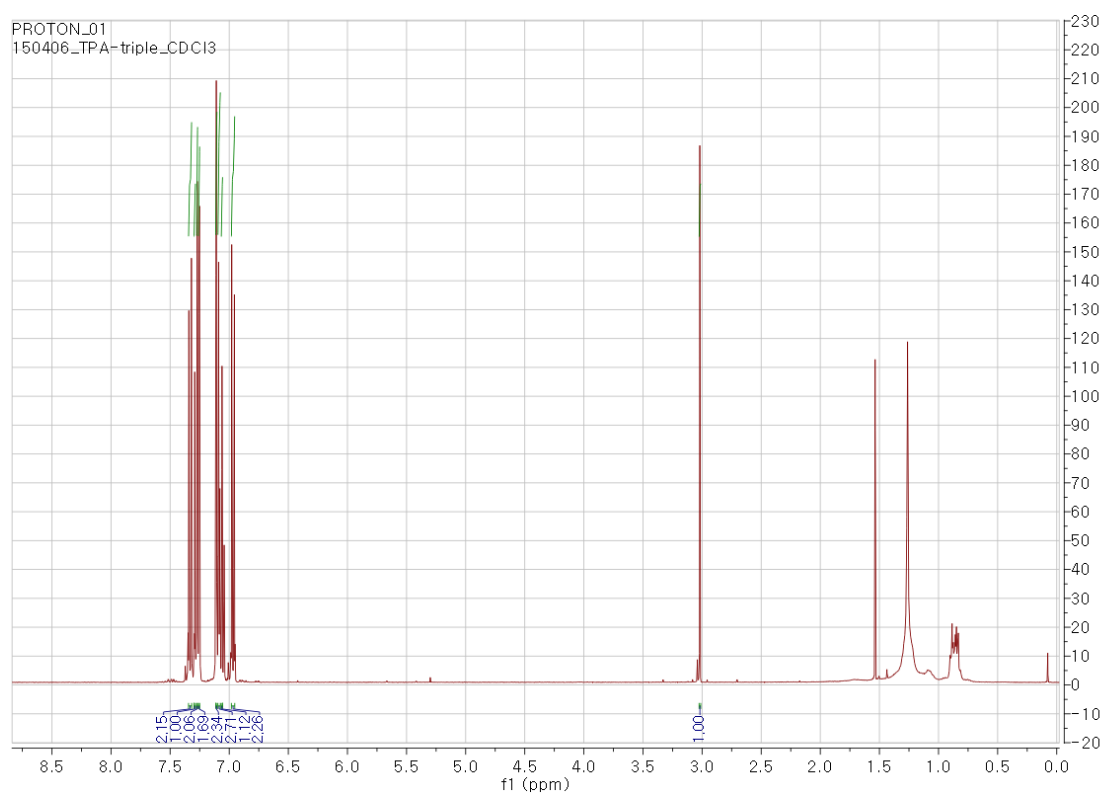


Figure 3.1 ^1H NMR of **D-1** in CDCl_3

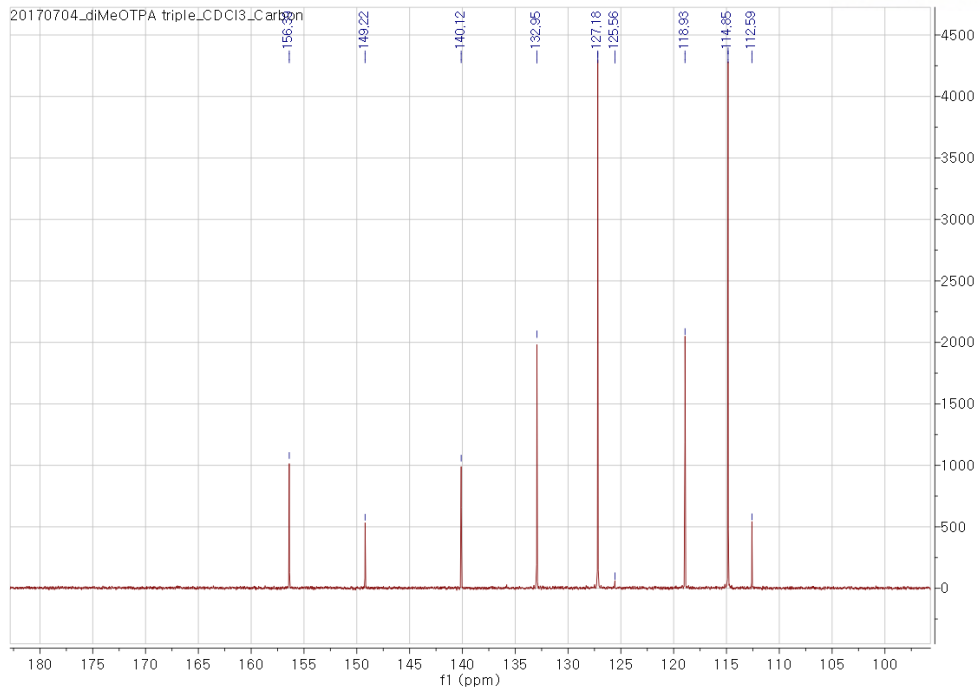


Figure 3.4 ^{13}C NMR of **D-2** in CDCl_3

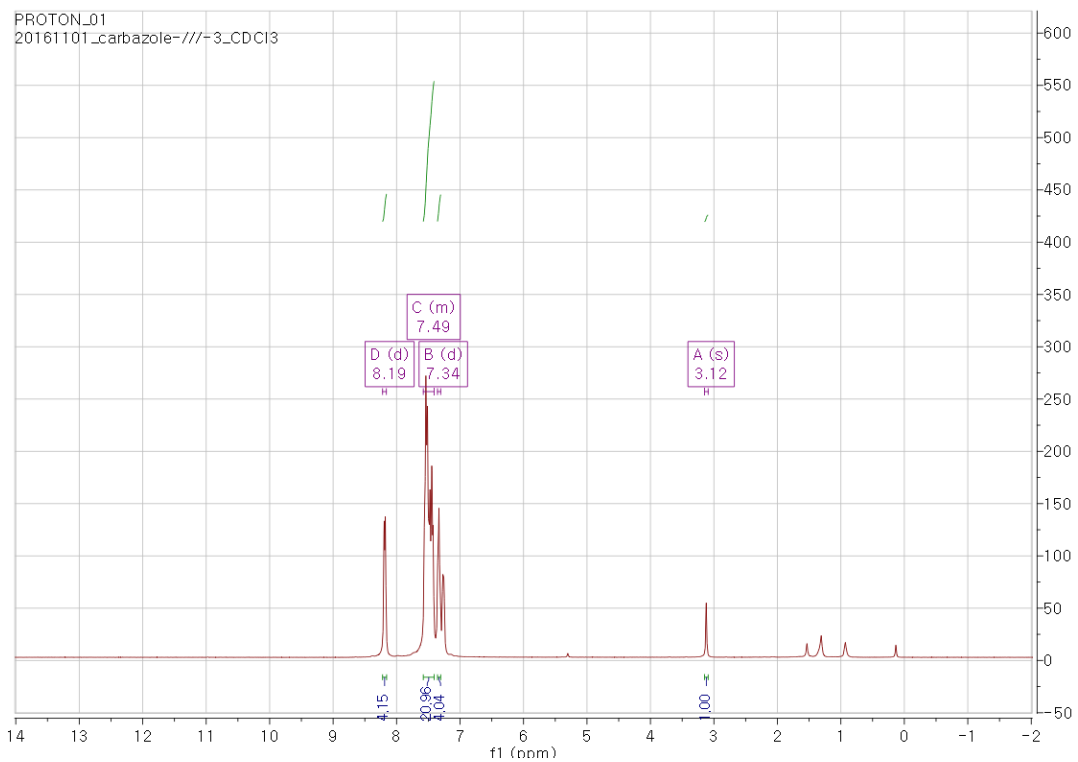


Figure 3.5 ^1H NMR of **D-3** in CDCl_3

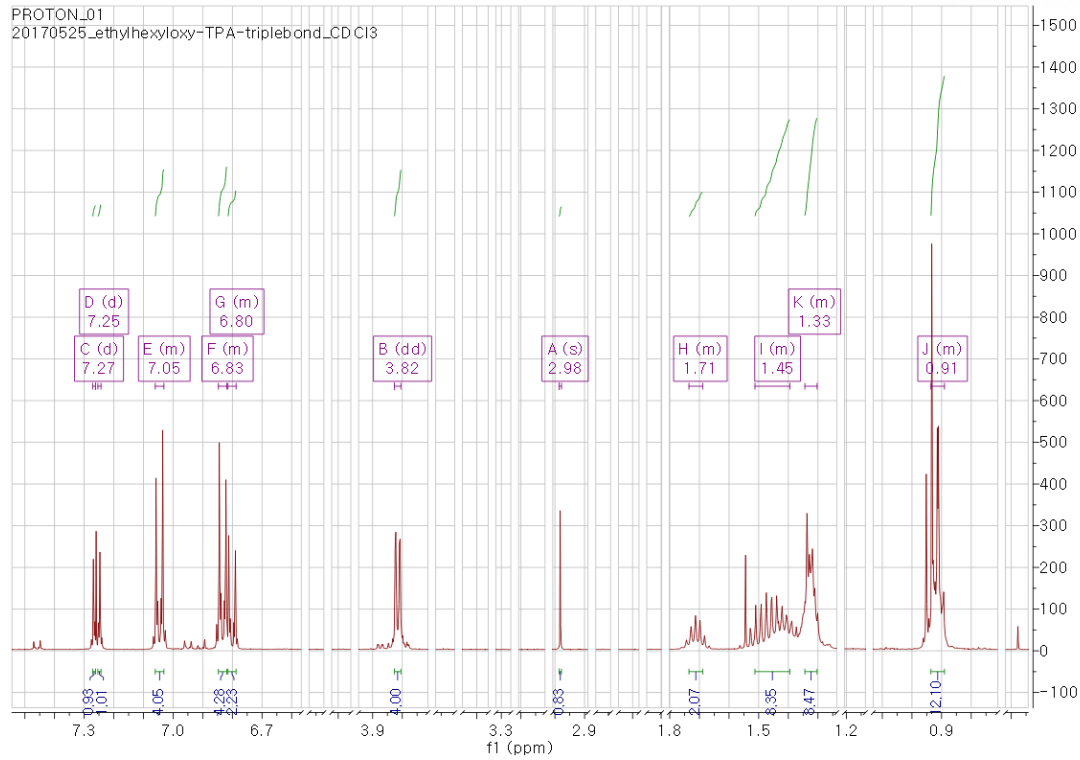


Figure 3.6 ^1H NMR of **D-4** in CDCl_3

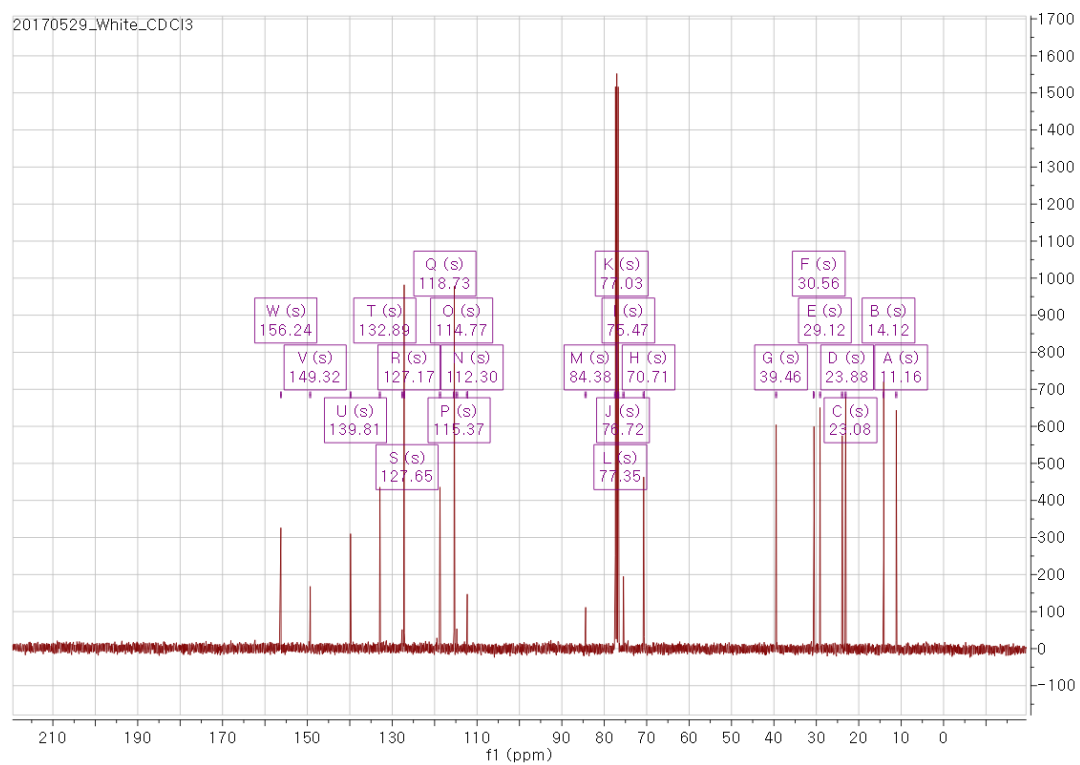


Figure 3.7 ^{13}C NMR of **D-4** in CDCl_3

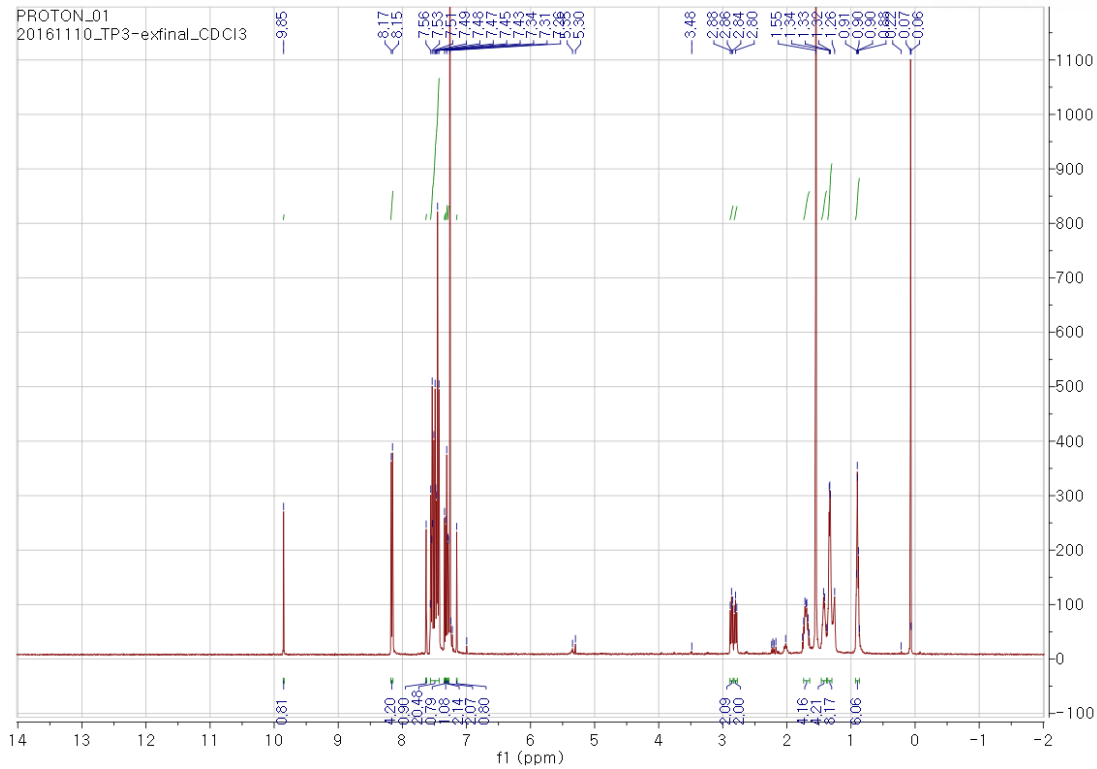


Figure 3.12 ^1H NMR of EF-3 in CDCl_3 adf

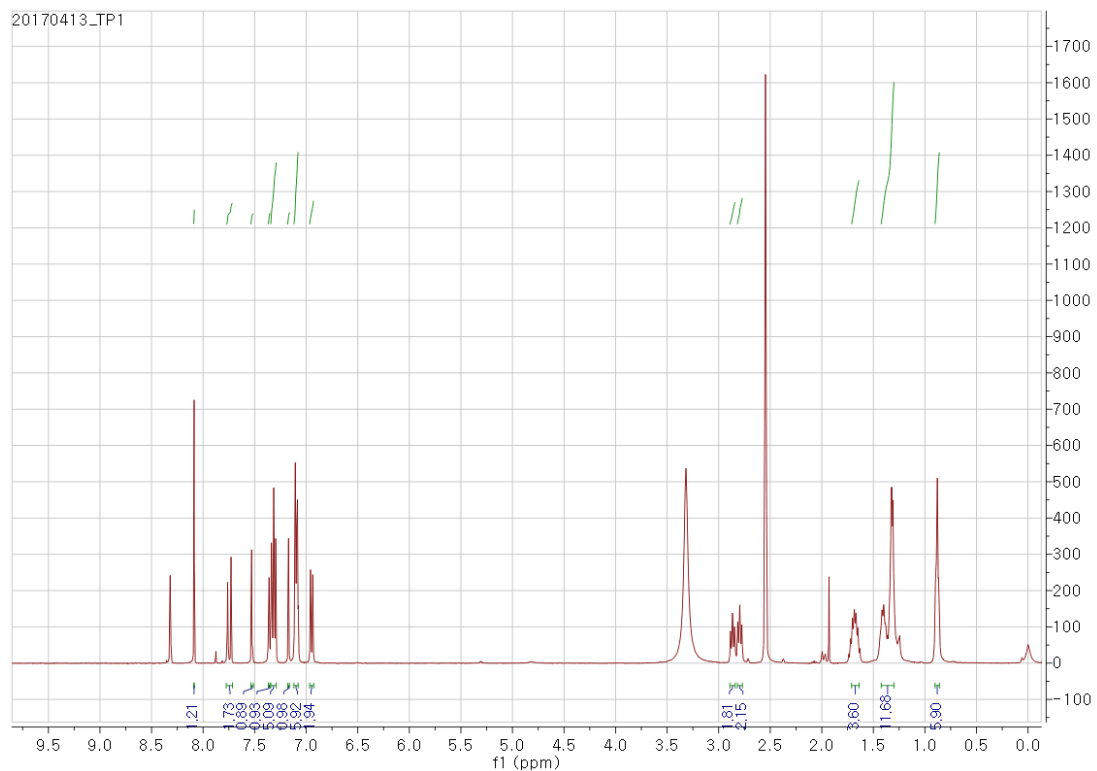


Figure 3.13 ^1H NMR of TP-1 in $\text{DMSO}/\text{CDCl}_3$

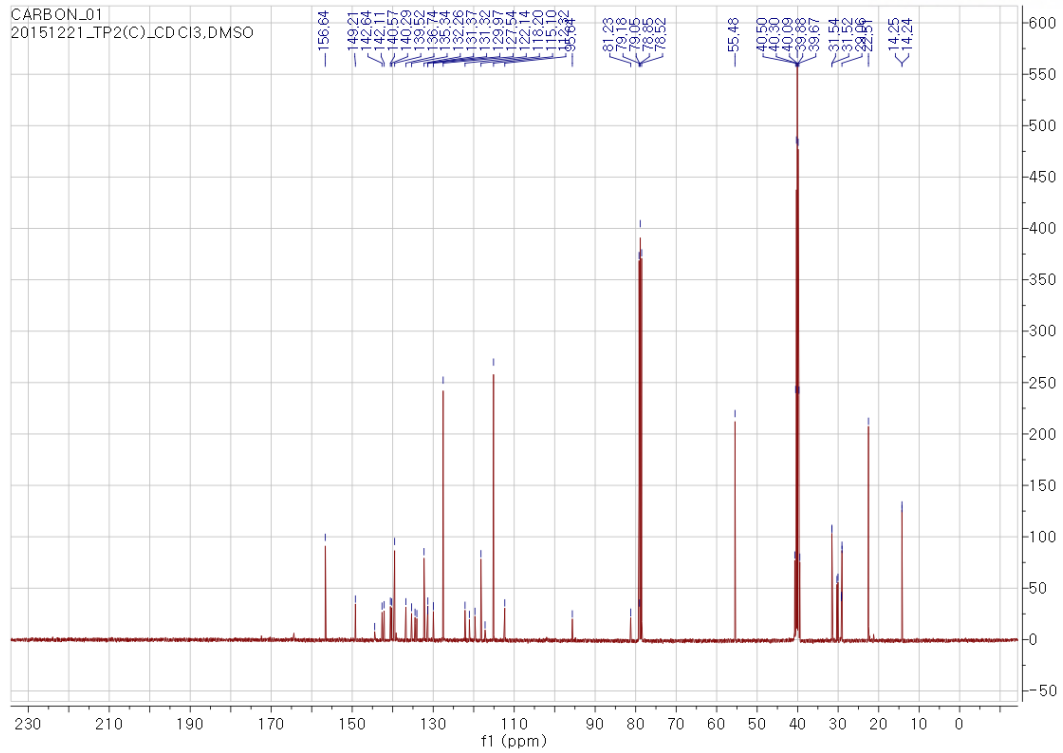


Figure 3.16 ^{13}C NMR of TP-2 in DMSO/ CDCl_3

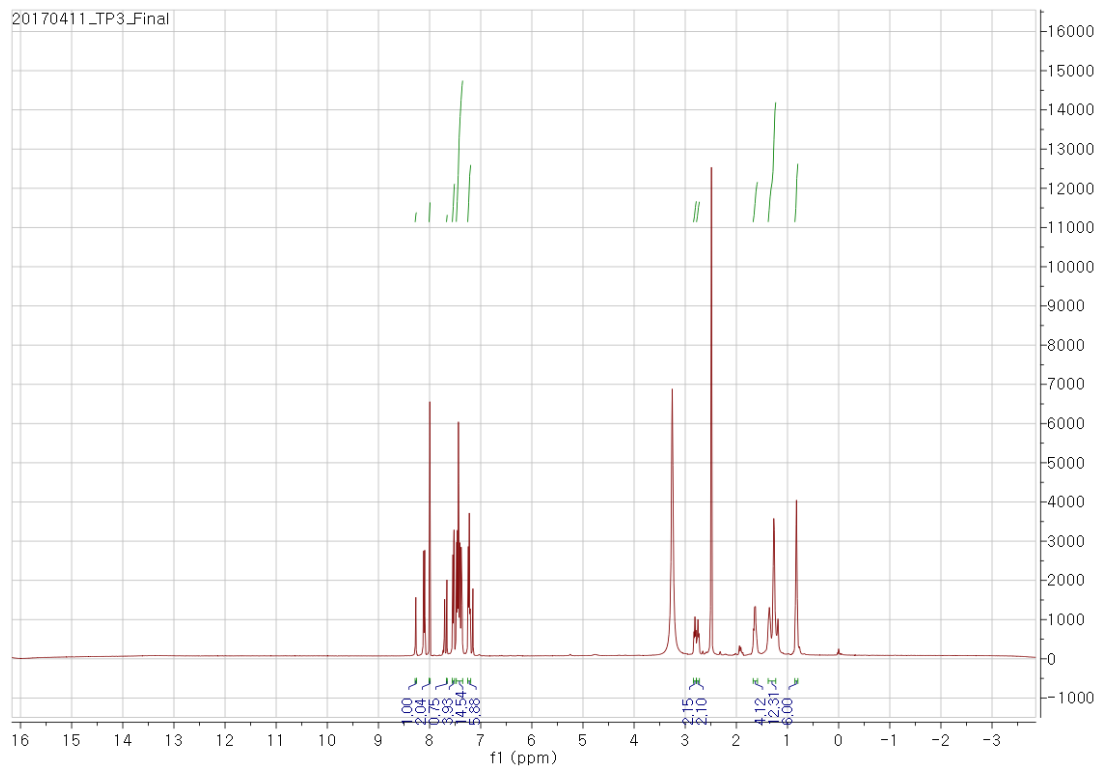
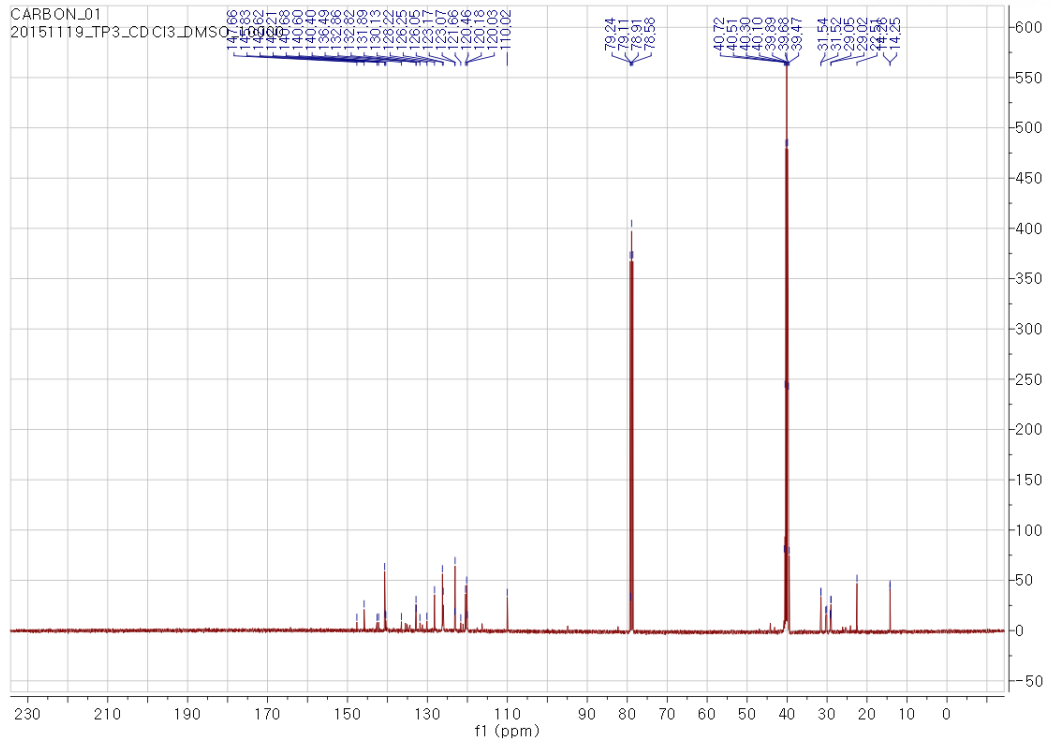


Figure 3.17 ^1H NMR of TP-3 in DMSO/ CDCl_3



3.2 Device Fabrication

3.2.1 DSC device fabrication

The photoanode and counter electrode were prepared on Fluorine-doped Tin Oxide glass (FTO, Nippon Sheet Glass Co., Ltd). In case of the photoanode, the substrates were cleaned with Acetone, Ethanol and Isopropanol for 10 min with a ultrasonic cleaner, and it also were treated by an UV ozone cleaning system for more hydrophilic substrate's surface and removing any contamination. After the cleaning process, a compact TiO₂ later was deposited on the FTO surface by soaking in the solution of 0.04 M aqueous TiCl₄ solution for 30 min at 70°C. After washed with DI water and Ethanol, the TiO₂ transparent layer was deposited on the substrate by a screen-printing method with a mask (MESH S/T250, Emulsion 12 μm). For conventional type cells with organic solvent electrolyte, 1.8 μm thickness transparent layer of 18 nm TiO₂ nanoparticles (Dongjin Semichem Co., Ltd) was prepared. For the celss with ionic liquid electrolyte, 3.5 μm thickness transparent layer of 8-10 nm TiO₂ nanoparticles (Ti-Nanoxide MC/SP, Solaronix). The all transparent layers coated 2.5 μm thickness second layer of scattering particles (Ti-Nanoxide R/SP, Solaronix) by the screen-printing method. The substrates with the printed TiO₂ layer was gradually sintered at 150°C for 10 min, 325°C for 5min, 327°C for 5 min, 450°C for 15 min, and 500°C for 30 min. After the sintering process and cooling to 80°C, the photoanode was immersed in the 0.04 M aqueous TiCl₄ solution for 30 min at 70°C. After washed with DI water and Ethanol, the photoanode was sintered again 500°C for 30 min. These photoanodes were immersed for 3 hours into a solution of 0.2 mM dye dissolved in a binary solvent of chloroform and ethanol (volume ratio, 7L3) with 10 mM chenodeoxycholic acid (CDCA) as co-adsorbate under dark condition. In case of TP-2 and TP-4, a binary solvent of chloroform, tert-butanol and acetonitrile (volume ratio, 2:9:9) was additionally used with 1 mM CDCA. For the counter electrodes, a FTO glasses were washed as same as the photoanode, and drilled by a hand drill for injecting of an electrolyte. The substrate was brushed with 10mM H₂PtCl₆ · 6H₂O ethanol solution, and sintered at 400°C for 15 min. These photoelectrode and counter electrode were assembled into a sandwich type cells by a 25 μm thick Surlyn films and sealed up by pressing at 110°C. The internal space of cells was perfused with an electrolyte by means of vacuum back filling, and the hole of injecting was sealed using the Surlyn films and a cover glass.

3.2.2 Electrolyte fabrication

The iodine electrolyte was consisted of 0.055 M I₂, 0.025 M LiI, 0.05 M guanidine thiocyanate (GuSCN), 0.6 M 1,2-dimethyl-3-propylimidazolium iodide and 0.5 M 4-*tert*-butylpyridine(TBP) in the acetonitrile and valeronitrile mixed solvent (volume ratio, 85:15). For ionic liquid electrolyte, a mixtures of 1-ethyl-3-methylimidazolium iodide (EMII), 1,3-dimethylimidazolium iodide (DMII) and 1-ethyl-3-methylimidazoliumtetracyanoborate(EMITCB) was used for enhance the properties of eutectic-based electrolyte. The composition of the ionic liquid electrolyte was as follow: DMII/EMII/EMITCB/I₂/TBP/GuSCN (molar ratio, 12:12:16:1.67:3.33:0.67). In addition, the commercial eutectic electrolyte (TDE-250, Solaronix) was used.

IV. Conclusion

We designed and synthesized total four organic sensitizers changing functional groups (proton, methoxy, carbazole and 2-ethylhexyloxy) on donor moieties. By varying the functional groups, we studied the suitability of functional group characteristics to three environmental factors (thermal, light and water) and enhanced the stability and PCE at thin TiO₂ film condition. In comparison with TP-1 without functional group, TP-2 with methoxy groups achieved high PCE and strong thermal stability but TP-2 was the most vulnerable to humidity because methoxy groups act as good donating group but hydrogen bonding between water and methoxy respectively. On the other hands, TP-3 showed the lowest PCE and thermal stability out of TP-series but TP-3 achieved the highest water stability due to twisted linkage to donor moiety and bulky form blocking water molecules respectively. In consideration of the characteristics of these functions, TP-4 with 2-ethylhexyloxy group was designed and synthesized to supplement water stability of TP-2 maintaining the high PCE of TP-2. As a result, relatively long alkyl chain of 2-ethylhexyloxy group improved water stability protecting oxygen of alkoxy group and keep the high PCE. Namely, molecular engineering for finding suitable functional groups affect both of PCE and stability so, it is necessary to recognize the importance of molecular engineering about diverse functional groups.

V. Reference

- LABORATORY, N. R. E. Best Research-Cell Efficiencies. <https://www.nrel.gov/pv/assets/images/efficiency-chart.png>.
- Oregan, B.; Gratzel, M., A Low-Cost, High-Efficiency Solar-Cell Based on Dye-Sensitized Colloidal TiO₂ Films. *Nature* **1991**, 353 (6346), 737-740.
- Freitag, M.; Teuscher, J.; Saygili, Y.; Zhang, X.; Giordano, F.; Liska, P.; Hua, J.; Zakeeruddin, S. M.; Moser, J. E.; Gratzel, M.; Hagfeldt, A., Dye-sensitized solar cells for efficient power generation under ambient lighting. *Nat Photonics* **2017**, 11 (6), 372-+.
- Ardo, S.; Meyer, G. J., Photodriven heterogeneous charge transfer with transition-metal compounds anchored to TiO₂ semiconductor surfaces. *Chem. Soc. Rev.* **2009**, 38 (1), 115-164.
- Hagfeldt, A.; Gratzel, M., Light-Induced Redox Reactions in Nanocrystalline Systems. *Chem. Rev.* **1995**, 95 (1), 49-68.
- Hagfeldt, A.; Boschloo, G.; Sun, L. C.; Kloo, L.; Pettersson, H., Dye-Sensitized Solar Cells. *Chem. Rev.* **2010**, 110 (11), 6595-6663.
- Zhu, K.; Neale, N. R.; Miedaner, A.; Frank, A. J., Enhanced charge-collection efficiencies and light scattering in dye-sensitized solar cells using oriented TiO₂ nanotubes arrays. *Nano Lett.* **2007**, 7 (1), 69-74.
- Yella, A.; Lee, H. W.; Tsao, H. N.; Yi, C. Y.; Chandiran, A. K.; Nazeeruddin, M. K.; Diao, E. W. G.; Yeh, C. Y.; Zakeeruddin, S. M.; Gratzel, M., Porphyrin-Sensitized Solar Cells with Cobalt (II/III)-Based Redox Electrolyte Exceed 12 Percent Efficiency. *Science* **2011**, 334 (6056), 629-634.
- Nakade, S.; Kanzaki, T.; Kubo, W.; Kitamura, T.; Wada, Y.; Yanagida, S., Role of electrolytes on charge recombination in dye-sensitized TiO₂ solar cell (1): The case of solar cells using the I-/I₃⁻ redox couple. *J. Phys. Chem. B* **2005**, 109 (8), 3480-3487.
- Mathew, S.; Yella, A.; Gao, P.; Humphry-Baker, R.; Curchod, B. F. E.; Ashari-Astani, N.; Tavernelli, I.; Rothlisberger, U.; Nazeeruddin, M. K.; Gratzel, M., Dye-sensitized solar cells with 13% efficiency achieved through the molecular engineering of porphyrin sensitizers. *Nat Chem* **2014**, 6 (3), 242-247.
- Molla, M. Z.; Mizukoshi, N.; Furukawa, H.; Ogomi, Y.; Pandey, S. S.; Ma, T.; Hayase, S., Transparent conductive oxide-less back contact dye-sensitized solar cells using cobalt electrolyte. *Prog. Photovoltaics* **2015**, 23 (9), 1100-1109.
- Yum, J. H.; Baranoff, E.; Kessler, F.; Moehl, T.; Ahmad, S.; Bessho, T.; Marchioro, A.; Ghadiri, E.; Moser, J. E.; Yi, C. Y.; Nazeeruddin, M. K.; Gratzel, M., A cobalt complex redox shuttle for dye-sensitized solar cells with high open-circuit potentials. *Nat Commun* **2012**, 3.
- Amadelli, R.; Argazzi, R.; Bignozzi, C. A.; Scandola, F., Design of Antenna-Sensitizer Polynuclear Complexes - Sensitization of Titanium-Dioxide with [Ru(Bpy)₂(Cn)₂]₂ru(Bpy(Coo)₂)₂⁻. *J. Am. Chem. Soc.* **1990**, 112 (20), 7099-7103.
- Nazeeruddin, M. K.; Splivallo, R.; Liska, P.; Comte, P.; Gratzel, M., A swift dye uptake procedure for dye sensitized solar cells. *Chem. Commun.* **2003**, (12), 1456-1457.
- Wang, P.; Zakeeruddin, S. M.; Moser, J. E.; Nazeeruddin, M. K.; Sekiguchi, T.; Gratzel, M., A stable quasi-solid-state dye-sensitized solar cell with an amphiphilic ruthenium sensitizer and polymer gel electrolyte (vol 2, pg 402, 2003). *Nat Mater* **2003**, 2 (7), 498-498.
- Nazeeruddin, M. K.; Kay, A.; Rodicio, I.; Humphrybaker, R.; Muller, E.; Liska, P.; Vlachopoulos, N.; Gratzel, M., Conversion of Light to Electricity by Cis-X₂bis(2,2'-Bipyridyl-4,4'-Dicarboxylate)Ruthenium(II) Charge-Transfer Sensitizers (X = Cl⁻, Br⁻, I⁻, Cn⁻, and Scn⁻) on Nanocrystalline TiO₂ Electrodes. *J. Am. Chem. Soc.* **1993**, 115 (14), 6382-6390.
- Sommeling, P. M.; Spath, M.; Smit, H. J. P.; Bakker, N. J.; Kroon, J. M., Long-term stability testing of dye-sensitized solar cells. *J Photoch Photobio A* **2004**, 164 (1-3), 137-144.
- Agrell, H. G.; Lindgren, J.; Hagfeldt, A., Degradation mechanisms in a dye-sensitized solar cell studied by UV-VIS and IR spectroscopy. *Sol Energy* **2003**, 75 (2), 169-180.

19. Mishra, A.; Fischer, M. K. R.; Bauerle, P., Metal-Free Organic Dyes for Dye-Sensitized Solar Cells: From Structure: Property Relationships to Design Rules. *Angew Chem Int Edit* **2009**, *48* (14), 2474-2499.
20. Imahori, H.; Umeyama, T.; Ito, S., Large pi-Aromatic Molecules as Potential Sensitizers for Highly Efficient Dye-Sensitized Solar Cells. *Acc. Chem. Res.* **2009**, *42* (11), 1809-1818.
21. Wang, X. F.; Tamiaki, H., Cyclic tetrapyrrole based molecules for dye-sensitized solar cells. *Energ Environ Sci* **2010**, *3* (1), 94-106.
22. Edvinsson, T.; Li, C.; Pschirer, N.; Schoneboom, J.; Eickemeyer, F.; Sens, R.; Boschloo, G.; Herrmann, A.; Mullen, K.; Hagfeldt, A., Intramolecular charge-transfer tuning of perylenes: Spectroscopic features and performance in Dye-sensitized solar cells. *J Phys Chem C* **2007**, *111* (42), 15137-15140.
23. Mahmood, A., Triphenylamine based dyes for dye sensitized solar cells: A review. *Sol Energy* **2016**, *123*, 127-144.
24. Wang, Z. S.; Cui, Y.; Dan-Oh, Y.; Kasada, C.; Shinpo, A.; Hara, K., Molecular Design of Coumarin Dyes for Stable and Efficient Organic Dye-Sensitized Solar Cells. *J Phys Chem C* **2008**, *112* (43), 17011-17017.
25. Lee, C. L.; Lee, W. H.; Yang, C. H., High Efficiency of Dye-Sensitized Solar Cells Based on Ruthenium and Metal-Free Dyes. *Int J Photoenergy* **2013**.
26. Ito, S.; Miura, H.; Uchida, S.; Takata, M.; Sumioka, K.; Liska, P.; Comte, P.; Pechy, P.; Graetzel, M., High-conversion-efficiency organic dye-sensitized solar cells with a novel indoline dye. *Chem. Commun.* **2008**, (41), 5194-5196.
27. Karthikeyan, S.; Lee, J. Y., Zinc-Porphyrin Based Dyes for Dye-Sensitized Solar Cells. *J. Phys. Chem. A* **2013**, *117* (42), 10973-10979.
28. Birel, O.; Nadeem, S.; Duman, H., Porphyrin-Based Dye-Sensitized Solar Cells (DSSCs): a Review. *J Fluoresc* **2017**, *27* (3), 1075-1085.
29. Haid, S.; Marszalek, M.; Mishra, A.; Wielopolski, M.; Teuscher, J.; Moser, J. E.; Humphry-Baker, R.; Zakeeruddin, S. M.; Gratzel, M.; Bauerle, P., Significant Improvement of Dye-Sensitized Solar Cell Performance by Small Structural Modification in pi-Conjugated Donor-Acceptor Dyes. *Adv. Funct. Mater.* **2012**, *22* (6), 1291-1302.
30. Tsao, H. N.; Yi, C.; Moehl, T.; Yum, J. H.; Zakeeruddin, S. M.; Nazeeruddin, M. K.; Gratzel, M., Cyclopentadithiophene Bridged Donor-Acceptor Dyes Achieve High Power Conversion Efficiencies in Dye-Sensitized Solar Cells Based on the tris-Cobalt Bipyridine Redox Couple. *Chemsuschem* **2011**, *4* (5), 591-594.
31. Zhou, D. F.; Cai, N.; Long, H. J.; Zhang, M.; Wang, Y. H.; Wang, P., An Energetic and Kinetic View on Cyclopentadithiophene Dye-Sensitized Solar Cells: The Influence of Fluorine vs Ethyl Substituent. *J Phys Chem C* **2011**, *115* (7), 3163-3171.
32. Zhang, L.; Cole, J. M., Anchoring Groups for Dye-Sensitized Solar Cells. *Acs Appl Mater Inter* **2015**, *7* (6), 3427-3455.
33. Chae, Y.; Kim, S. J.; Kim, J. H.; Kim, E., Metal-free organic-dye-based flexible dye-sensitized solar textiles with panchromatic effect. *Dyes Pigm.* **2015**, *113*, 378-389.
34. Jin, M. Y.; Kim, B. M.; Jung, H. S.; Park, J. H.; Roh, D. H.; Nam, D. G.; Kwon, T. H.; Ryu, D. H., Indoline-Based Molecular Engineering for Optimizing the Performance of Photoactive Thin Films. *Adv. Funct. Mater.* **2016**, *26* (38), 6876-6887.
35. Qin, C. J.; Wong, W. Y.; Han, L. Y., Squaraine Dyes for Dye-Sensitized Solar Cells: Recent Advances and Future Challenges. *Chem-Asian J* **2013**, *8* (8), 1706-1719.
36. Yang, H. Y.; Yen, Y. S.; Hsu, Y. C.; Chou, H. H.; Lin, J. T., Organic Dyes Incorporating the Dithieno[3,2-b:2',3'-d]thiophene Moiety for Efficient Dye-Sensitized Solar Cells. *Org. Lett.* **2010**, *12* (1), 16-19.
37. Zhu, E. W.; Ni, B.; Zhao, B. F.; Hai, J. F.; Bian, L. Y.; Wu, H. B.; Tang, W. H., Synthesis and Photovoltaic Characterization of Dithieno[3,2-b:2',3'-d]thiophene-Derived Narrow-Bandgap Polymers. *Macromol. Chem. Phys.* **2014**, *215* (3), 227-234.

38. Qin, H.; Wenger, S.; Xu, M.; Gao, F.; Jing, X.; Wang, P.; Zakeeruddin, S. M.; Gratzel, M., An organic sensitizer with a fused dithienothiophene unit for efficient and stable dye-sensitized solar cells. *J. Am. Chem. Soc.* **2008**, *130* (29), 9202-+.
39. Roh, D. H.; Kim, K. M.; Nam, J. S.; Kim, U. Y.; Kim, B. M.; Kim, J. S.; Kwon, T. H., Strategy for Improved Photoconversion Efficiency in Thin Photoelectrode Films by Controlling pi-Spacer Dihedral Angle. *J Phys Chem C* **2016**, *120* (43), 24655-24666.
40. Kwon, T. H.; Armel, V.; Nattestad, A.; MacFarlane, D. R.; Bach, U.; Lind, S. J.; Gordon, K. C.; Tang, W. H.; Jones, D. J.; Holmes, A. B., Dithienothiophene (DTT)-Based Dyes for Dye-Sensitized Solar Cells: Synthesis of 2,6-Dibromo-DTT. *J. Org. Chem.* **2011**, *76* (10), 4088-4093.
41. Quesada, E.; Taylor, R. J. K., One-pot conversion of activated alcohols into terminal alkynes using manganese dioxide in combination with the Bestmann-Ohira reagent. *Tetrahedron Lett.* **2005**, *46* (38), 6473-6476.
42. Proteau-Gagne, A.; Rochon, K.; Roy, M.; Albert, P. J.; Guerin, B.; Gendron, L.; Dory, Y. L., Systematic replacement of amides by 1,4-disubstituted[1,2,3] triazoles in Leu-enkephalin and the impact on the delta opioid receptor activity. *Bioorg. Med. Chem. Lett.* **2013**, *23* (19), 5267-5269.
43. Teng, C.; Yang, X. C.; Yang, C.; Tian, H. N.; Li, S. F.; Wang, X. N.; Hagfeldt, A.; Sun, L. C., Influence of Triple Bonds as pi-Spacer Units in Metal-Free Organic Dyes for Dye-Sensitized Solar Cells. *J Phys Chem C* **2010**, *114* (25), 11305-11313.
44. Arakawa, Y.; Kang, S.; Watanabe, J.; Konishi, G., Assembly of thioether-containing rod-like liquid crystalline materials assisted by hydrogen-bonding terminal carboxyl groups. *Rsc Advances* **2015**, *5* (11), 8056-8062.
45. Wang, Q.; Moser, J. E.; Gratzel, M., Electrochemical impedance spectroscopic analysis of dye-sensitized solar cells. *J. Phys. Chem. B* **2005**, *109* (31), 14945-14953.
46. Ambrose, J. F.; Nelson, R. F., Anodic Oxidation Pathways of Carbazoles .1. Carbazole and N-Substituted Derivatives. *J. Electrochem. Soc.* **1968**, *115* (11), 1159-&.
47. Morin, J. F.; Leclerc, M.; Ades, D.; Siove, A., Polycarbazoles: 25 years of progress. *Macromol. Rapid Commun.* **2005**, *26* (10), 761-778.
48. Chen, C.; Yang, X. C.; Cheng, M.; Zhang, F. G.; Sun, L. C., Degradation of Cyanoacrylic Acid-Based Organic Sensitizers in Dye-Sensitized Solar Cells. *Chemsuschem* **2013**, *6* (7), 1270-1275.
49. Yang, H. Y.; Hong, Y. T.; Kim, S., Catalytic enantioselective Friedel-Crafts alkylations of indoles with alpha '-phosphoric enones. *Org. Lett.* **2007**, *9* (12), 2281-2284.
50. De Simone, F.; Saget, T.; Benfatti, F.; Almeida, S.; Waser, J., Formal Homo-Nazarov and Other Cyclization Reactions of Activated Cyclopropanes. *Chem-Eur J* **2011**, *17* (51), 14527-14538.

VI. Acknowledgement

짧지만 길었던 E.R. Lab 에서의 대학원생 생활이 끝이 나고 졸업을 하게 되었습니다. 그동안 저를 지도해주신 권태혁 교수님께 감사의 말씀 전해드립니다. 학부 시절부터 지금까지 교수님께서 많은 조언과 격려로 힘을 내어 대학원 생활을 무사히 마무리할 수 있었습니다. 감사드립니다.

그리고 언제나 저를 믿고 기다려주신 어머니, 아버지 그리고 오빠에게 감사드립니다. 가족들 모두의 응원으로 대학원 공부를 끝까지 할 수 있었습니다. 특히나 부모님께서 저의 단단한 기둥이 되어주셔서 제가 흔들리지 않고 원하는 길을 찾아 나아갈 수 있었습니다. 정말 많은 의지가 되고 힘이 되었습니다. 감사합니다.

대학원에서 생긴 새로운 가족, 우리 E.R. Lab 멤버들 모두 고맙습니다. 정수 오빠, 현규 오빠, 병만 오빠, 현오 오빠, 현탁 오빠, 광민, 준혁, 덕호, 정승, 민수, 채현, 채규, 은혜, 왕효, 민규 모두와 함께 즐겁고 힘든 시간을 보내면서 너무나도 많은 정이 생겨버렸습니다. 먼저, 만형인 정수 오빠, 오빠에게 처음으로 유기합성을 배우고 성장할 수 있었습니다. 감사합니다. 현규 오빠는 오빠지만 친구같이 스스럼이 없이 대해 주셔서 항상 고마웠습니다. 무뚝뚝한 부산 사나이 같지만 알고 보면 따뜻한 남자인 병만 오빠, 오빠에게 DSC 에 관해서 많이 배울 수 있었습니다. 감사드립니다. 그리고 케미 폭발하는 형제 현오 오빠, 현탁 오빠 랩장으로서 랩실을 대표해 많은 일을 해내신다고 고생하셨습니다. 앞으로도 E.R Lab 을 위해서 힘내세요. 또한, 일을 너무 잘하는 동생들 덕호와 정승, 동생이지만 연구에 관해서는 너희들에게 많이 배울 수 있었어. 끝까지 열심히 해서 좋은 결과를 내기를 바라. Co-worker 준혁아, 함께 DSC 에 대해서 연구한다고 고생이 많았어. 끝까지 함께 좋은 논문을 완성해보자. 그리고 동생이지만 동생 같지 않은 민수야 나랑 놀아준다고 고생이 많았지. 너랑 이야기하면서 노는 게 참 재밌었는데 나 졸업했다고 잊으면 안 돼. 그리고 기나긴 홍일점 생활의 마침표를 찍게

해준, 은혜, 채규야 고마워. 가끔 셋이 모여서 이야기하면 서로의 이야기가 공감도 되고
흥미롭고 재밌었어. 랩실에 와서, 괜찮은 여동생들 사귄 수 있어서 난 참 운이 좋은
사람인 것 같아. 끝까지 열심히 해서 멋진 박사가 되길 바랄게. 그리고 채채은 시리즈의
첫째 채헌아, 둘째와 셋째 채규와 은혜와 함께 멋진 박사가 되길 바라. 그리고 내 동생
왕효, 선배로서 합성에 관해서 많은 걸 가르쳐주고 싶었고 그동안의 함께한 시간이
도움이 되었을까 모르겠네. 내가 없어도 합성 잘해야 한다. 누나가 응원할게.

마지막으로 대학원 생활 동안 도움을 주신 교수님께 감사드리며 응원해준 친구들, 선배,
동생들 모두에게 고마운 말을 전합니다.